Supplementary Material

Network organization of the human autophagy system

Christian Behrends, Mathew E. Sowa, Steven P. Gygi, and J. Wade Harper

Part 1. Supplementary Methods

Part 2. Supplementary Figures S1-S13

Part 3. Supplementary Tables S1-S7

Part 1. Supplementary Methods

Data Processing and Analysis. Mass spectral data was processed using *CompPASS*, as previously described[1] with modifications discussed below. Briefly, Sequest summary files were processed into a high threshold dataset based on a 2% protein false-positive rate by keeping the XCorr thresholds for each charge state constant while varying the ΔCn (thresholds: XCorr 2+ ≥ 2.5; XCorr 3+ ≥ 3.2; XCorr 4+ ≥ 3.5; +1 charge states were not collected). These processed data sets were merged for each duplicate run and used to populate a "stats table" consisting of each dataset for the AIN as well as 102 unrelated proteins (Dubs and their selected HCIPs[1]; https://harper.hms.harvard.edu/*CompPASS*_Dubs.html). The D^N-score and Z-score are calculated from total spectral counts (TSCs) for each protein found in association with each bait.

Because *CompPASS* was originally designed for analysis of mostly non-reciprocal datasets, we devised a new weighted D^N-score (WD^N-score) (Supplementary Fig. S2), which aids in the identification of HCIPs that are associated with multiple baits in a network. WD^N-scores were calculated as:

$$WD_{i,j} = \sqrt{(\lambda\omega_j)^p (x_{i,j})} \qquad \text{(Eq. 1)}$$

$$\lambda = \left(\frac{k}{\sum_{i=1}^{i=k} f_{i,j}}\right), \quad f_{i,j} = \begin{cases} 1 \,;\, X_{i,j} > 0 \\ X_{i,j} \end{cases} \qquad \text{(Eq. 2)}$$

$$\omega_j = \left(\frac{\sigma_j}{\overline{X}_j}\right), \quad \overline{X}_j = \frac{\sum_{i=1,\, j=n}^{i=k} X_{i,j}}{k} \quad ; n = 1,2,\ldots m \qquad \text{(Eq. 3)}$$

$X_{i,j}$ = total peptides for interactor j from bait i

$p = \begin{cases} \text{number of replicates} \\ \text{runs in which} \\ \text{the interactor is present} \end{cases}$

where ω_j is the weight factor for interactor j (Eq. 3), σ_j is the standard deviation of the TSCs for interactor j and the raw WD-score is divided by the threshold WD-score determined in the same manner as for the D-score described previously [1]. The previously described D-score is Eq. 1 without ω_j. The analyzed files, the primary output from *CompPASS*, were used for all analysis described here. As described below, we found significant interconnectivity in the network. Proteins identified in each LC-MS/MS experiment with a WD^N-scores ≥ 1 and a p-value ≤ 4.9×10^{-6} are considered HCIPs.

Comparison of HCIP abundance.

In order to compare the abundance of HCIPs found in the wild type and mutant ATG8 protein IP-MS/MS experiments we used the normalized spectral abundance factor (NSAF) approach previously applied to determine the abundance of proteins found in IP-

MS/MS datasets[2]. For each interactor in each IP-MS/MS experiments, the NSAF was calculated and then difference in NSAF values for that protein in wild type control and mutant experiment was determined. In order to plot the data using the $\log_2$ values of this difference while maintaining the proper sign of the value (positive for increase and negative for decrease), the conventional NSAF was multiplied by 100,000 so that each value was ≥ 1 before taking the $\log_2$ of the difference.

Gene Ontology Analysis of the AIN and ATG8 networks.

Gene Ontology (GO) process analysis was performed on both the HCIPs (WD^N-score > 1.0) from the AIN and separately for the HCIPs from the ATG8 sub network using in-house software. GO process terms were manually grouped into 25 broad categories for simplicity (Supplemental Table S7). HCIPs from each IP-MS/MS experiment were assigned a broad GO category where a single HCIP could have multiple category assignments, but only 1 per category. A final table of broad GO terms (Using the March 6, 2010 release) and their percentage found across all HCIPs was generated. This was repeated for non-HCIP proteins as well and was used to generate a mean and standard deviation for each broad GO category, representing the values found for each in the background protein dataset. GO term values for HCIPs were compared to these background values and p-values were calculated (Supplemental Fig. S5a). We feel that this method better reflects the enrichment of GO terms in our data rather than using the distributions for GO terms found across the entire human proteome because our IP-MS/MS procedure does not truly randomly sample all proteins in the proteome. Indeed, inspection of GO enrichment for background proteins shows that GO terms relating to canonical background proteins (such as “folding”, “translation”, and “cytoskeleton”) are significantly enriched in our background data when compared to the expected values for the human proteome (Supplemental Fig. S5a).

Part 2. Supplementary Figure Legends

Figure S1. Autophagy proteins and yeast autophagy signaling modules. a, Primary and secondary baits examined in this study organized by functional class. **b-e**, Diagrams of central signaling pathways in the autophagy system in budding yeast, including the Atg1 pathway (**b**), the Vps34 lipid kinase pathway (**c**), the UBL (Atg8/Atg12) conjugation pathway (**d**), and the vesicle recycling complex involving the transmembrane protein Atg9 and the peripheral membrane proteins Atg18, Atg2, and Atg27 (**e**). Yeast proteins are indicated by symbols. Mammalian orthologs for Atg8 are indicated. Adapted from: Levine, B. and Kroemer, G. (2008) Cell 132, 161.

Figure S2. Development of a weighted D^N-score for analysis of proteomic data within a collection of overlapping sub-networks. To better determine likely interacting proteins that are abundant across IP-MS/MS datasets, we developed a weighted D^N-score (WD^N-score) based on the observation that the standard deviation of the TSCs for known common interactors was much higher than that of known background proteins (expressed as %σ in panel **a**) (see Detailed Methods). **b,** A closer look at the distribution of proteins with %σ ≥ 100% versus those with %σ < 100% shows that proteins in this former category are rarely found in multiple IP-MS/MS experiments. **c,** Examples of proteins known to be background (FUS and ALDH1B1) versus proteins known to be true interactors (VCP and CUL3) shows the differences in the TSC distributions and the large %σ for the known interactors. **d,** Incorporating this information into the weighted D^N-score (see Detailed Methods) allows for 11% more proteins to be considered HCIPs versus using the previously describe D^N-score [1] indicating that most

abundant proteins remain designated as background. **e**, The total spectal counts (orange) for autophagy network bait proteins are plotted together with the number of HCIPs for each bait (in green) based on WD^N-score.

Figure S3. Global analysis of the autophagy interaction network. **a**, Heat map generated from hierarchical clustering of the 2553 proteins identified by LC-MS/MS for 65 autophagy network components without filtering via *CompPASS* [1]. The color of the interacting protein in the plot corresponds to its WD^N-score. **b**, Hierarchical clustering of 763 high-confidence interacting proteins after processing via *CompPASS*.

Figure S4. Development of a module within *CompPASS* to collapse networks using available protein interaction databases and its application to the autophagy interaction network (AIN). **a**, Since the nature of the interactions identified in our IP-MS/MS data cannot be determined to be either direct or indirect, we chose to analyze these interactions at a more conservative level by collapsing known multimeric protein complexes (present in BIOGRID, MINT and STRING) into a single representative node. For example, if the 6 proteins known to form a complex are found as HCIPs for a given bait, it cannot be determined to which of these 6 the bait directly interacts. Therefore, rather than reporting 6 interactions for this bait, we report a single interaction to a known protein complex comprised of those 6 interacting proteins. In this manner, we feel that we are not over-representing the number of interactions and can also better report associations with known protein complexes. **b**, Summary of novel and known interactions found using the *Network Collapse* function in *CompPASS* (panel **a**).

Figure S5. Functional and structural analysis of the autophagy interaction network. **a**, Enrichment of Gene Ontology (GO) process descriptors for HCIPs (WD^N-score ≥1.0, $p < 10^{-5}$) in the autophagy interaction network (AIN, left panel), the ATG8 sub-network (center panel), and proteins with WD^N-scores ≥ 1.0 (right panel). Enrichments were determined as described in the Supplemental Methods section. **b**, Hierarchical clustering of proteins found associated with 65 bait proteins, with the number of PFAM domains present indicated by the heat map. **c**, Distribution of PFAM domains found among baits (red bars) and HCIPs (blue bars). **d**, Analysis of hubs in the AIN. Hubs were identified based on their presence as HCIPs in IP-MS/MS experiments from 3 different baits with WD^N-Score ≥3 each and an average WD^N-Score ≥2 acrcoss all IP-MS/MS experiments in which a hub candidate was present based on TSCs. Primary and secondary bait refers to the classification in Fig 1.

Figure S6. Summary of reciprocal interactions for the AIN and analysis of previously reported interactions for the UBL conjugation system. a, Summary of the LC-MS/MS data for the UBL conjugation system showing the number of HCIPs, number of known interacting proteins in BIOGRID and MINT, and the number of reciprocal interactions observed. **b**, Summary of previously reported interaction for the UBL conjugation system. **c**, Summary of reciprocal interactions in the networks presented in Fig. 2 and Fig. 3 determined by LC-MS/MS. **d**, Merged interaction maps of HCIPs found in ≥ 2 IP-MS/MS experiments among indicated baits. Common interacting proteins with sub-threshold WD^N-scores were included if HCIP criteria were fulfilled in ≥ 1 IP-MS/MS experiment. **e**, Individual interaction maps showing all the HCIPs identified for primary and secondary baits examined in this study. Dotted lines indicate interactions found in BIOGRID, MINT, and STRING protein interaction databases. **f**, IP-Western validation. Myc-tagged interactors indicated were transfected into 293T cells with stable expression of indicated Flag-HA-bait or Flag-HA-GFP. Lysates were immunoprecipitated

with anti-myc resin and immunoblotted with either HA or anti-MYC antibodies. **g**, α-LC3 blot of 293T cells in the absence and present of Torin1 (200 nM, 3h), Rapamycin (200nM, 3h) and Bafilomycin (100 nM, 3h).

Figure S7. Summary of core interactions in the budding yeast autophagy system. All network data is based on BIOGRID and MINT databases. **a**, UBL conjugation system. **b**, Vps34p lipid kinase network. **c**, Atg1p protein kinase network. **d**, Atg2p membrane trafficking network. The corresponding human proteins are identified on the right of each panel. The color code indicates the type of interaction data.

Figure S8. Summary of LC-MS/MS data and comparison to existing protein interaction data for the core autophagy signaling systems, as well as for the ATG8 sub-network. **a**, The bait, number of HCIPs, number of novel interactions found, ratio of known and total interactions found, and the results of reciprocal LC-MS/MS of selected interacting proteins is shown for the ATG8 network. **b**, PFAM analysis of the ATG8 sub-network. Proteins containing the indicated PFAM protein interaction domains are shown.

Figure S9. Association of GST-ATG8 proteins with MYC-tagged interacting proteins. **a-b**, Vectors expressing the indicated MYC-tagged HCIPs for the ATG8 network were transfected into 293T cells and subsequently tested for interaction with GST-ATG8 proteins. After extensive washing of GST-ATG8 resin, associated proteins were detected by immunoblotting with anti-MYC antibodies. **c**, *Ex vivo* validation. MYC-tagged proteins in extracts from 293T cells were tested for GST-ATG8 binding *in vitro* (Panel a). Green: binding. Red: no binding observed. Extracts from 293T cells transiently expressing the indicated Mys-tagged ATG8 interacting protein were lysed and extracts subjected to in vitro binding with the indicated GST-ATG8 isoform purified from bacteria. Washed complexes were subjected to SDS-PAGE, and immunoblotted using anti-MYC antibodies. **d**, Summary of binding data.

Figure S10. Association of GST-ATG8 proteins with *in vitro* translated interacting proteins. **a**, The indicated HCIPs for ATGs were translated and ^{35}S-methionine-labelled *in vitro* using reticulocyte extracts. **b**, Five μl of translation product was incubated in 150 μl of binding buffer containing 2 μg of the indicated GST-ATG8 protein bound to 10 μl of GSH-Sepharose beads. After incubation for 1 hour, beads were washed 5 times with 1 ml of binding buffer. Associated proteins were separated by SDS-PAGE, stained with Coomassie, and subjected to autoradiography. **c**, Summary table indicating the proteins that interact with each ATG8 ortholog *in vitro*.

Figure S11. LIR-dependence of interactions between GST-ATG8 proteins and in vitro translated HCIPs. **a**, Immobilized GST (lane 1), GST-GABARAP (lane 2), GST-GABARAP Y49A/L50A (lane 3) or GST-GABARAP R70A (lane 4) were analyzed for binding with the indicated HCIPs as described in Figure S10. **b**, Immobilized GST (lane 1), GST-MAP1LC3B (lane 2), GST-MAP1LC3B F52A/L53A (lane 3) or GST-MAP1LC3B R70A (lane 4) were analyzed for binding with the indicated HCIPs as described in Figure S10. **c**, Structure of the SQSTM1 (p62) LIR-motif (cyan) bound to the LDS of MAP1LC3B (green) (pdb code: 2K6Q). Mutations employed in the experiments in panel **b** are shown: R70A (yellow), F52A (red), L53A (purple). **d**, Effect of the R70A mutation in MAP1LC3B on interaction with the ATG8 sub-network. Red edges, no interaction; green edges, interaction unaffected; blue edges, interaction reduced or eliminated. **e**, Phylogenetic tree for Atg18p and Atg21p related proteins from humans (Hs), S. pombe (Sp), C. elegans (Ce), Drosophila (Dm), and S. cerevisiae (Sc).

Figure S12. Proteomic analysis of the ATG8 sub-network: Effect of C-terminal glycine on protein interactions *in vivo*. Effect of deletion of the C-terminal glycine residue from ATG8 proteins. The primary data is provided in Supplemental Table S3a and S3b. The indicated ATG8 proteins or their C-terminal ΔGly counterparts, were purified from 293T cells and subjected to LC-MS/MS. TSCs were used to calculate differential interaction scores using a modified version of the NSAF method (see Detailed Methods for method of the scoring). Only scores for proteins that passed the stringent threshold for statistical significance are highlighted (red, increased abundance; blue, decreased abundance).

Figure S13. RNAi analysis of genes in the autophagy interaction network. **a**, Representative images of GFP-MAPLC3B expressing U2OS cells after transfection with the indicated siRNAs in the presence and absence of Rapamycin (200 nM, 6h). DRAQ5 is used to mark nuclei. The GFP images are the same as those used in Fig. 5a in the main paper. **b**, Normalized integrated spot signal per cell (N-ISSC) for U2OS cells expressing GFP-MAP1LC3B either alone or 6 h after treatment with rapamycin or Torin1 (200 nM). **c**, α-LC3 blot of U2OS cells with the indicated treatments. **d**, Representative images of GFP-GABARAP expressing U2OS cells after transfection with the indicated siRNAs in the presence. DRAQ5 is used to mark nuclei. **e**, ISSC values for cells transfected with 296 siRNAs targeting 74 genes. **f**, Normalized ISSC (N-ISSC) for GFP-GABARAP with or without Rapamycin (6 h) (4 siRNAs/gene). Unless noted otherwise, $p < 0.01$ using Students T-test; *, $p<0.05$; white rectangles, $p>0.05$. **g**, Quantitative RT-PCR results for depletion of the indicated genes in U2OS cells. Error bars, Standard Deviation, n = 3. **h**, Validation of siRNA mediated depletion of CDC37, PDCD6IP, PI4K2A, ATG12, ATG5, and NEDD4. Four siRNAs targeting the indicated genes were transfected into U2OS cells and after 72 h, cells were lysed and probed with antibodies against the indicated proteins. Blots were re-probed with PCNA as a loading control. All antibodies were from Cell Signaling Technologies, with the exception of anti-PI4K2A, which was from Novus. **i**, Validation of flow cytometry flux assay. Color-coding for histogram and bar-graph correspond. GFP-MAP1LC3B U2OS cells or empty U2OS cells were subjected to flow cytomety. The mean fluorescence intensity (MFI) was determined using FLOWJO. Torin1 activated flux through the autophagy pathway and this was reversed by BafA1 treatment. Error bars, Standard Deviation, n = 2.

Part 3. Supplementary Tables S1-S7

Table S1. cDNA constructs.

Table S2. Primary LC-MS/MS data for 65 baits in the autophagy interaction network.

Table S3. Primary LC-MS/MS data for the ATG8 sub-network with and without the C-terminal Gly residue. (Sheet 1 and 2).

Table S4. Primary LC-MS/MS data for sub-network proteomic analysis with and without Torin1 treatment. (Sheet 1 and 2).

Table S5. siRNA and RT-PCR primer sequences used in this study.

Table S6. Normalized average intensity spot signals/cell for the RNAi autophagosome formation screen.

Table S7. Curation of Genes lacking Gene Ontology Process descriptors (Sheet 2), as well as the GO categories employed for this analysis (Sheet 1).

References

1. Sowa, M. E., Bennett, E. J., Gygi, S. P. & Harper, J. W. Defining the human deubiquitinating enzyme interaction landscape. Cell 138, 389-403 (2009).
2. Sardiu, M. E. et al. Probabilistic assembly of human protein interaction networks from label-free quantitative proteomics. Proc Natl Acad Sci U S A 105, 1454-1459 (2008).

Supplementary Fig. S1

a

	Primary bait	Secondary bait
ULK1 kinase network	ULK1 ULK2	C12orf44 CAMKK2 FOXO3A GBL KIAA0652 PRKAA1 PRKAA2 PRKAB1 PRKAB2 PRKAG1 PRKAG2 RB1CC1 STK11
PIK3C3-BECN1 network	PIK3C3 BECN1 UVRAG AMBRA	DDA1 KIAA0831 NRBF2
SH3GLB1 network	SH3GLB1	KLHDC10 SH3GLB2
ATG2-WIPI network	ATG2A WIPI1 WIPI2	WDR45
UBL conjugation system	ATG3 ATG4B ATG4C ATG5 ATG7 ATG10 ATG12 ATG16L1	TECPR1
Human ATG8's	GABARAP GABARAPL1 GABARAPL2 MAP1LC3A MAP1LC3B MAP1LC3C	FYCO1 GBAS KBTBTD7 NEK9 NSMAF PIK3C2A PIK3CG RABGAP1 RASSF5 SQSTM1 STK3 STK4 UBA5
Vesicle trafficking	CLN3 GOSR1 NSF RAB24	
Miscellaneous	DDIT3 HIF1A PDPK1 TRAF2	

b

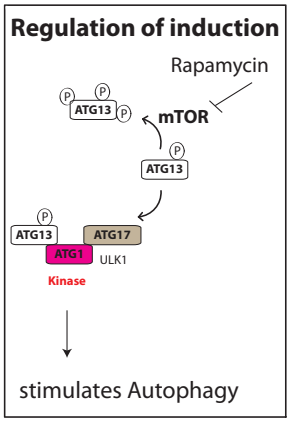

c

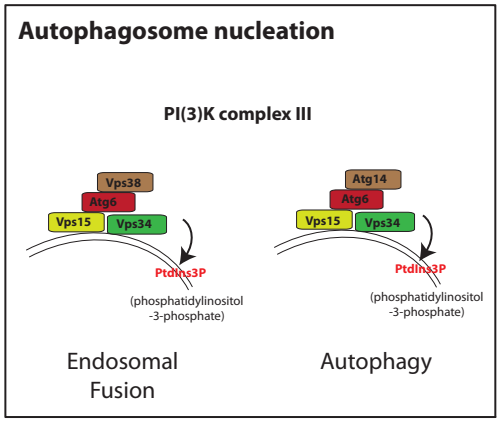

d

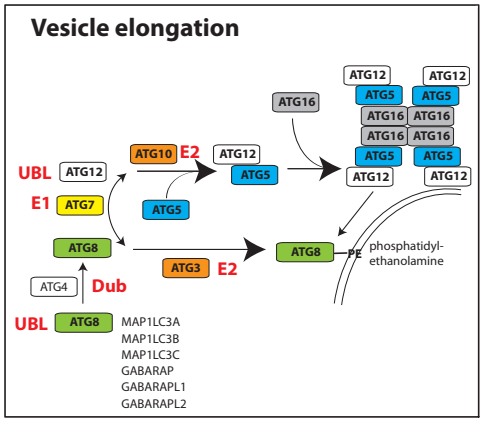

e

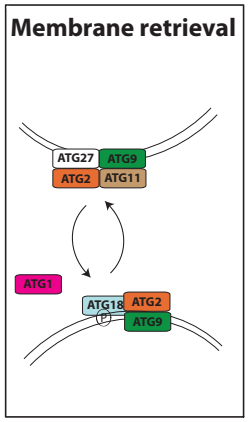

Supplementary Fig. S2

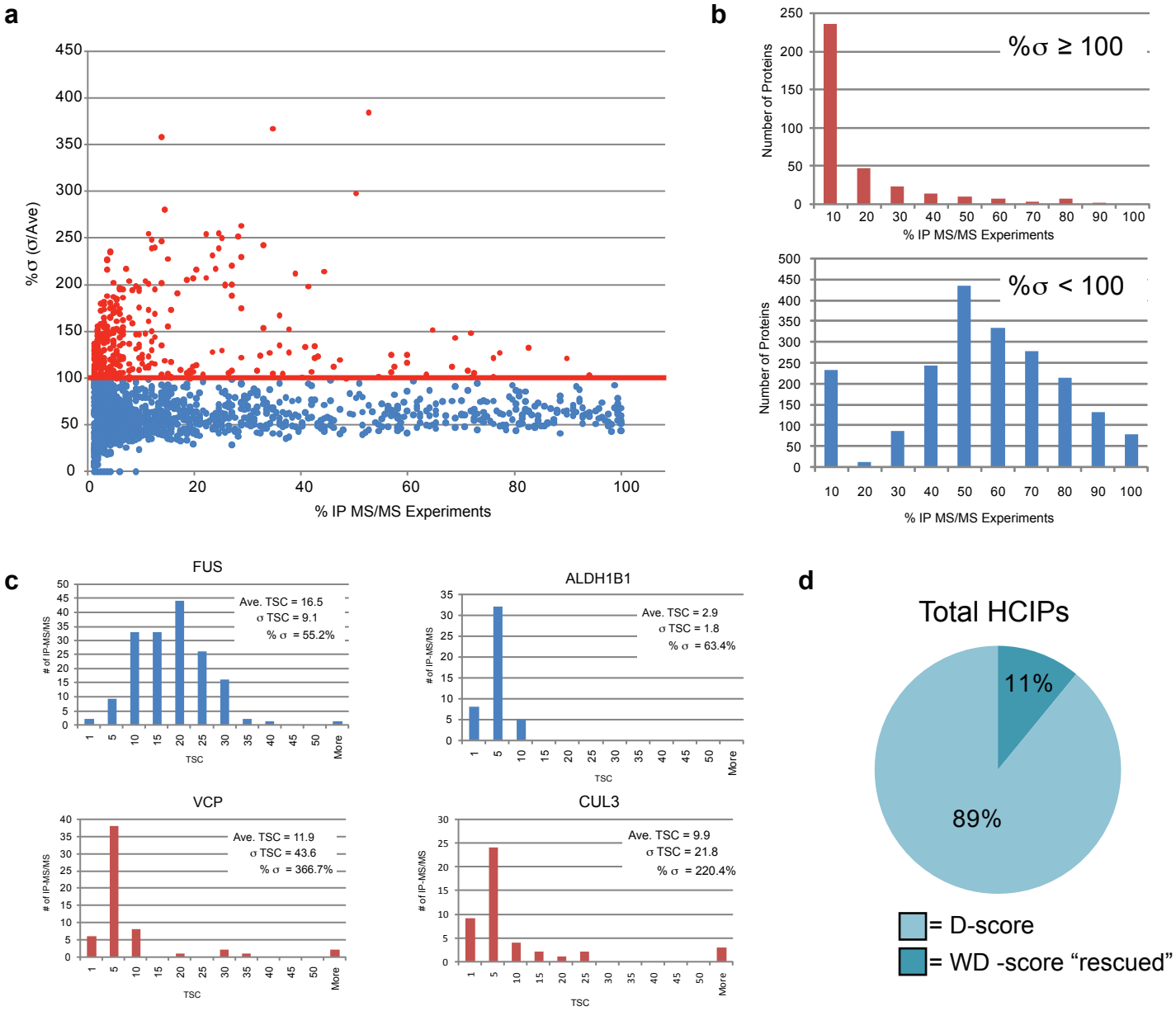

e

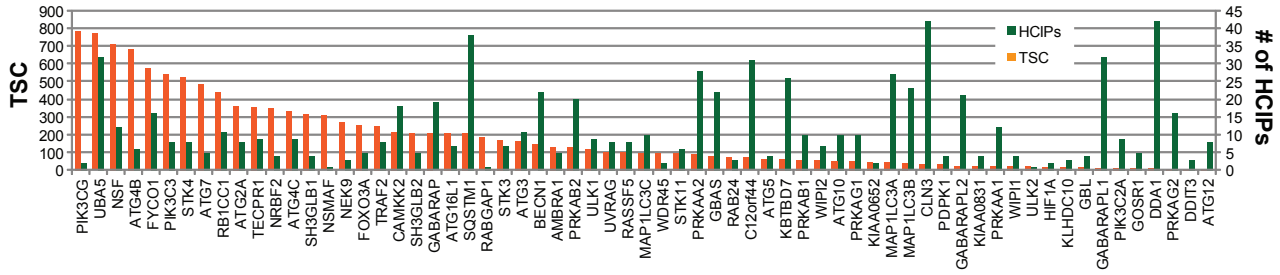

Supplementary Fig. S3

a All interacting proteins

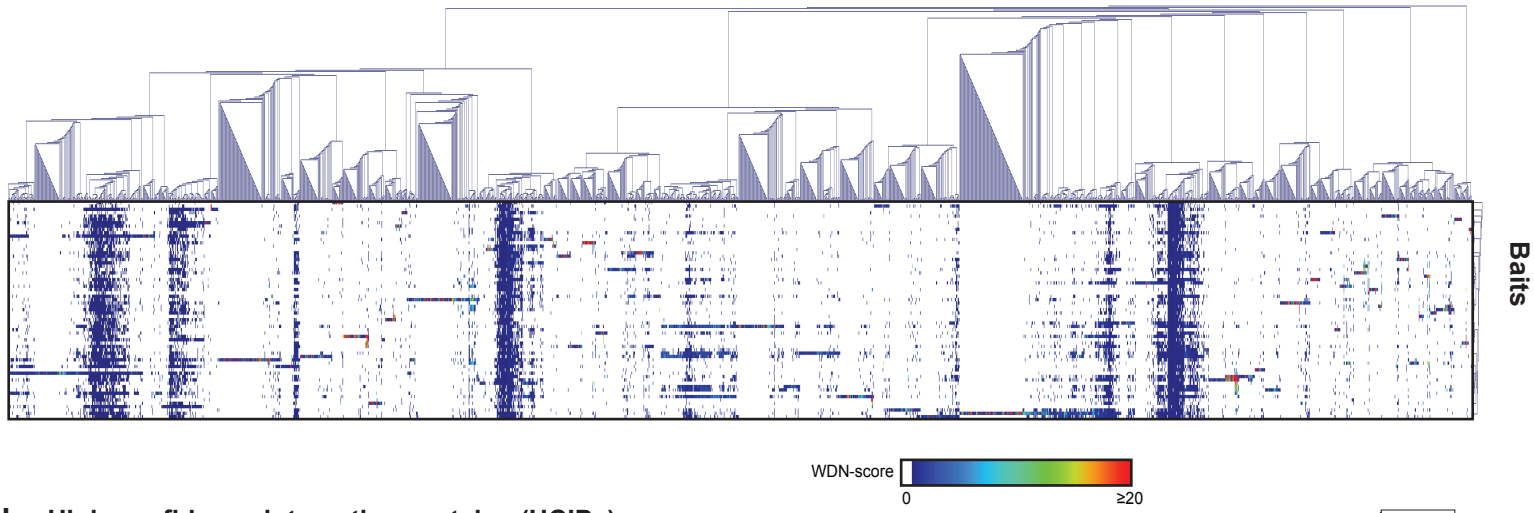

b High-confidence interacting proteins (HCIPs)

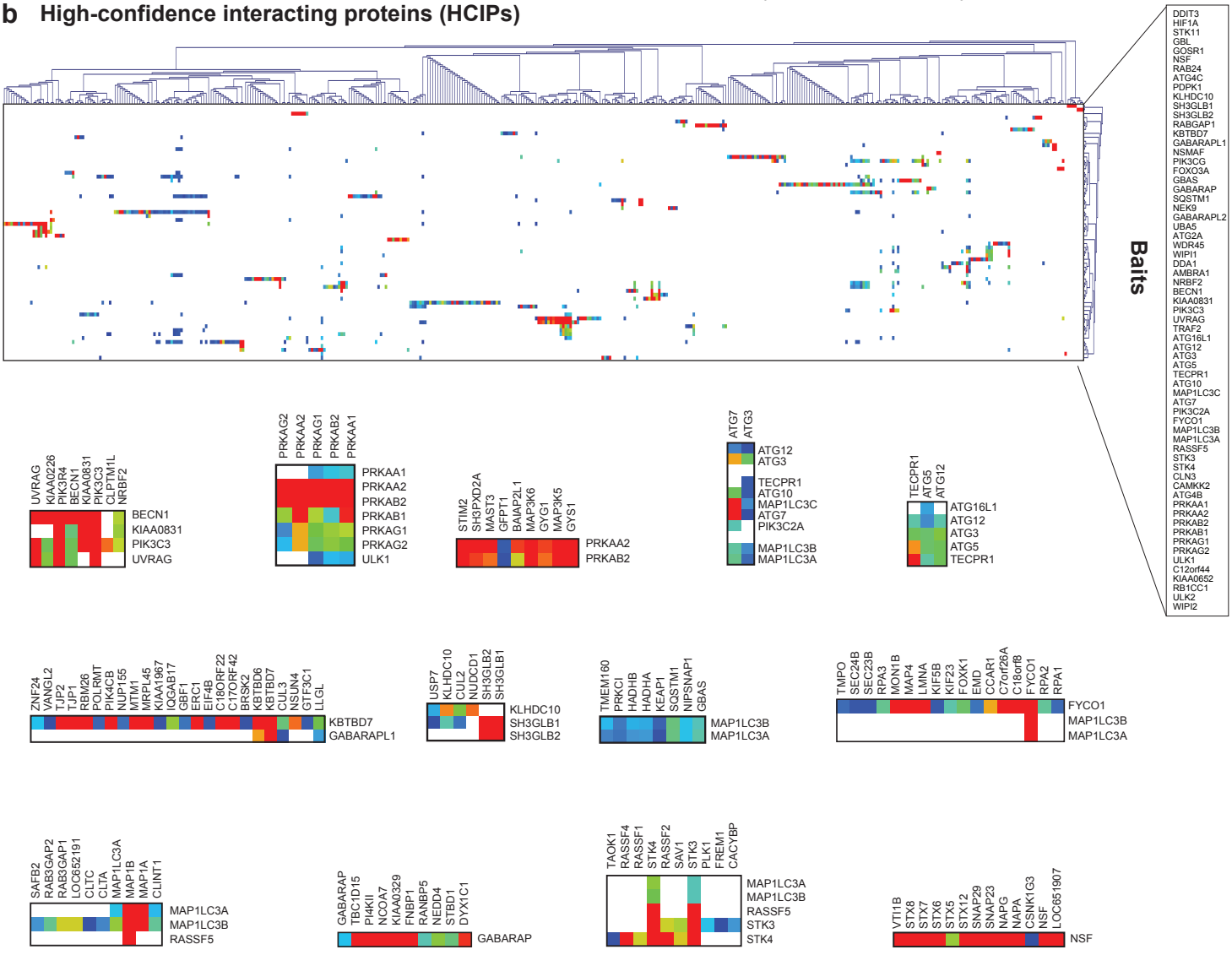

Supplementary Fig. S4

a

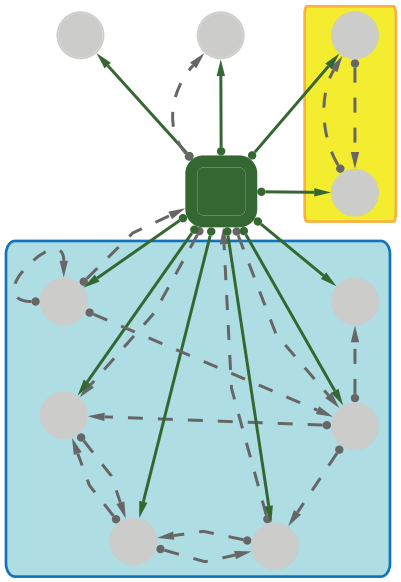

Raw

Total # of associations	10
Total # of known complexes	2
Total # of known bait-prey associations	5
Total # of novel bait-prey associations	5

Collapse Network using known protein complexes

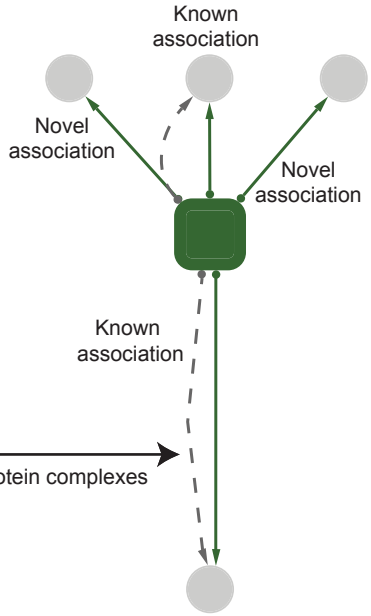

Adjusted

Total # of associations	4
Total # of known complexes	2
Total # of known bait-prey associations	2
Total # of novel bait-prey associations	2

= PPI database interaction (MINT, BioGRID, STRING)

= MS/MS association

= MS/MS bait

= HCIP for bait

b

Type of Interaction	Total Number	
HCIPs	751	**Raw Network**
Known Protein Complexes (KPC)	84	
Known Bait-KPC Interactions	40	
Total Associations	497	**Collapsed Network**
Known Bait-HCIP/KPC Associations	68	
Novel Bait-HCIP Associations	429	

Supplementary Fig. S5

a

Complete AIN Network

Broad GO Category Process	AIN HCIPs % found	Background Proteins % found	Background Proteins σ	p-value
DNA Damage	1.99%	2.93%	0.52%	3.57E-02
DNA Replication	0.71%	0.91%	0.90%	4.14E-01
GTPase Signaling	0.90%	0.43%	0.39%	1.14E-01
Ion/AA Transport	0.76%	1.24%	0.58%	2.03E-01
Macroscopic Cellular Response	4.84%	5.63%	0.70%	1.28E-01
OTHER	5.32%	10.24%	0.87%	6.86E-09
Protein/AA modifiction	2.47%	1.06%	0.89%	5.73E-02
RNA Processing	1.90%	8.45%	2.83%	1.02E-02
apoptosis	4.99%	4.55%	0.64%	2.47E-01
biosynthetic	6.08%	4.05%	1.22%	4.82E-02
chromatin	1.38%	1.71%	0.54%	2.70E-01
cytoskeleton	1.99%	2.37%	0.45%	2.00E-01
development	7.79%	8.41%	1.16%	2.95E-01
folding	3.13%	4.54%	1.04%	8.77E-02
metabolism & catabolism	8.07%	7.25%	1.83%	3.26E-01
mitosis	4.23%	5.13%	0.59%	6.37E-02
morphogenesis	1.85%	1.05%	0.36%	1.25E-02
phosphorylation	5.46%	1.83%	0.64%	5.59E-09
protein localization and transport	8.02%	7.03%	0.71%	8.11E-02
proteolysis	4.27%	1.46%	0.59%	1.02E-06
signal transduction	6.74%	4.07%	0.64%	1.36E-05
transcription	4.84%	4.61%	1.00%	4.09E-01
translation	2.23%	7.57%	2.37%	1.23E-02
ubiquitin	2.71%	1.15%	1.07%	7.41E-02
vesicle transport	7.31%	2.34%	0.86%	3.39E-09

significant increase
significant decrease
no significant change

ATG8 Sub-Network

Broad GO Category Process	ATG8 Network HCIPs % found	Background Proteins % found	Background Proteins σ	p-value
DNA Damage	0.76%	2.93%	0.52%	1.48E-05
DNA Replication	0.00%	0.91%	0.90%	1.56E-01
GTPase Signaling	2.04%	0.43%	0.39%	2.18E-05
Ion/AA Transport	0.76%	1.24%	0.58%	2.05E-01
Macroscopic Cellular Response	5.34%	5.63%	0.70%	3.38E-01
OTHER	4.33%	10.24%	0.87%	4.49E-12
Protein/AA modifiction	4.33%	1.06%	0.89%	1.28E-04
RNA Processing	0.25%	8.45%	2.83%	1.87E-03
apoptosis	5.85%	4.55%	0.64%	2.08E-02
biosynthetic	5.60%	4.05%	1.22%	1.02E-01
chromatin	0.00%	1.71%	0.54%	7.56E-04
cytoskeleton	2.54%	2.37%	0.45%	3.49E-01
development	6.87%	8.41%	1.16%	9.16E-02
folding	0.51%	4.54%	1.04%	5.05E-05
metabolism & catabolism	6.87%	7.25%	1.83%	4.18E-01
mitosis	1.78%	5.13%	0.59%	7.39E-09
morphogenesis	1.78%	1.05%	0.36%	2.05E-02
phosphorylation	4.83%	1.83%	0.64%	1.14E-06
protein localization and transport	11.45%	7.03%	0.71%	2.96E-10
proteolysis	6.11%	1.46%	0.59%	2.22E-15
signal transduction	6.87%	4.07%	0.64%	5.50E-06
transcription	4.58%	4.61%	1.00%	4.87E-01
translation	0.00%	7.57%	2.37%	7.15E-04
ubiquitin	4.83%	1.15%	1.07%	3.03E-04
vesicle transport	11.70%	2.34%	0.86%	0.00E+00

significant increase
significant decrease
no significant change

AIN Network Background Proteins*

Broad GO process Category	Background Proteins %Found	Whole Proteome %Found	Whole Proteome s	p-value
DNA Damage	2.95%	1.67%	0.57%	1.21E-02
DNA Replication	0.86%	0.38%	0.13%	1.08E-04
GTPase Signaling	0.43%	2.33%	0.79%	8.17E-03
Ion/AA Transport	1.22%	2.54%	0.86%	6.33E-02
Macroscopic Cellular Response	5.63%	6.78%	2.31%	3.09E-01
OTHER	10.32%	27.40%	9.32%	3.34E-02
Protein/AA modifiction	1.04%	0.78%	0.27%	1.59E-01
RNA Processing	8.62%	2.00%	0.68%	0.00E+00
apoptosis	4.59%	2.71%	0.92%	2.05E-02
biosynthetic	4.01%	2.24%	0.76%	1.01E-02
chromatin	1.72%	0.83%	0.28%	7.98E-04
cytoskeleton	2.39%	1.06%	0.36%	1.11E-04
development	8.38%	12.03%	4.09%	1.86E-01
folding	4.61%	0.77%	0.26%	0.00E+00
metabolism & catabolism	7.21%	5.99%	2.04%	2.75E-01
mitosis	5.16%	4.39%	1.49%	3.04E-01
morphogenesis	1.03%	1.38%	0.47%	2.30E-01
phosphorylation	1.80%	2.26%	0.77%	2.73E-01
protein localization and transport	6.99%	2.90%	0.99%	1.71E-05
proteolysis	1.41%	1.65%	0.56%	3.38E-01
signal transduction	3.97%	7.00%	2.38%	1.02E-01
transcription	4.64%	6.52%	2.22%	1.98E-01
translation	7.68%	0.80%	0.27%	0.00E+00
ubiquitin	1.12%	1.03%	0.35%	3.94E-01
vesicle transport	2.22%	2.57%	0.87%	3.44E-01

significant increase
significant decrease
no significant change

*background proteins have a WD^N-score < 1 and a TSC p-value > 3E-5

b

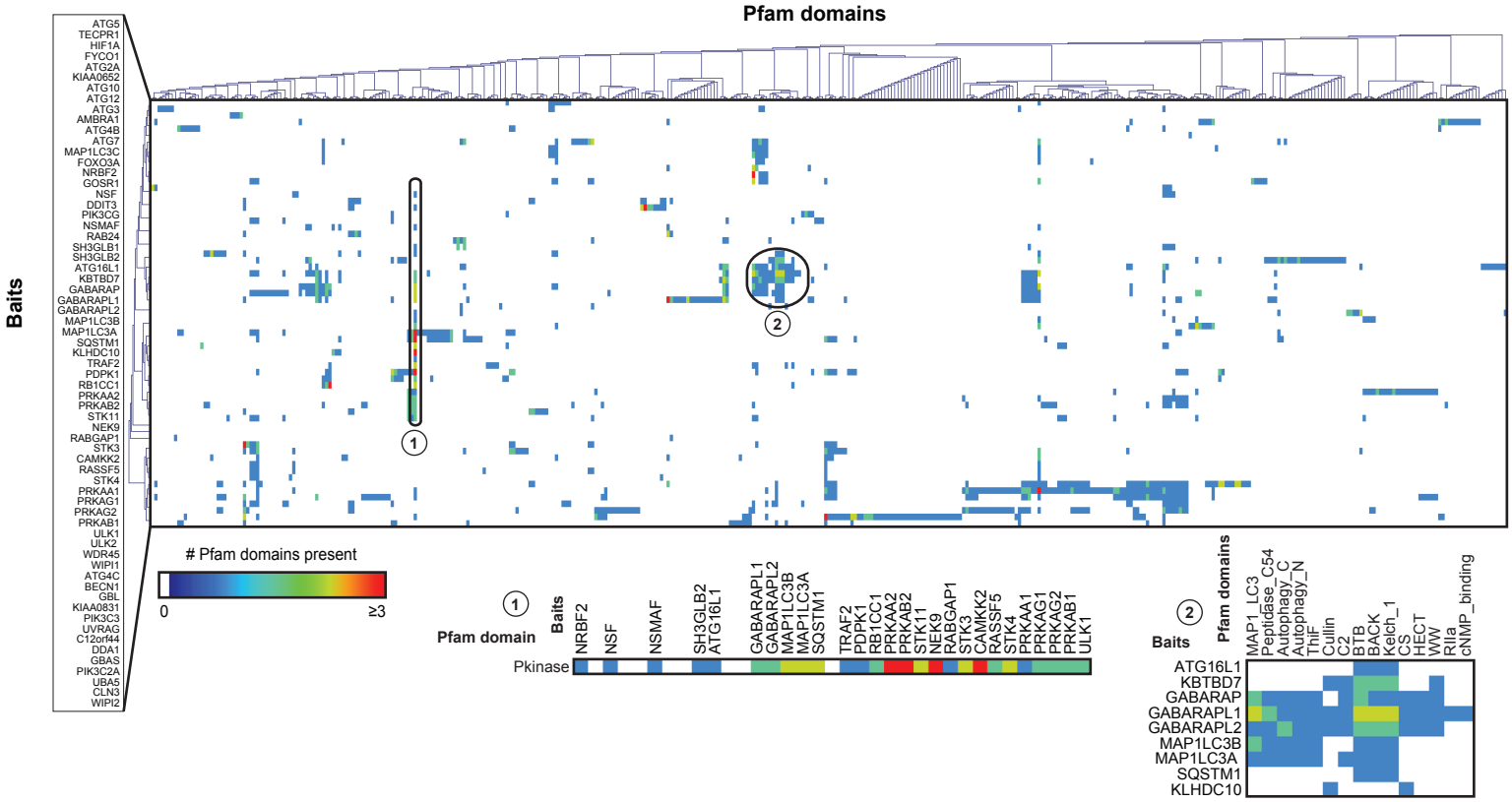

c

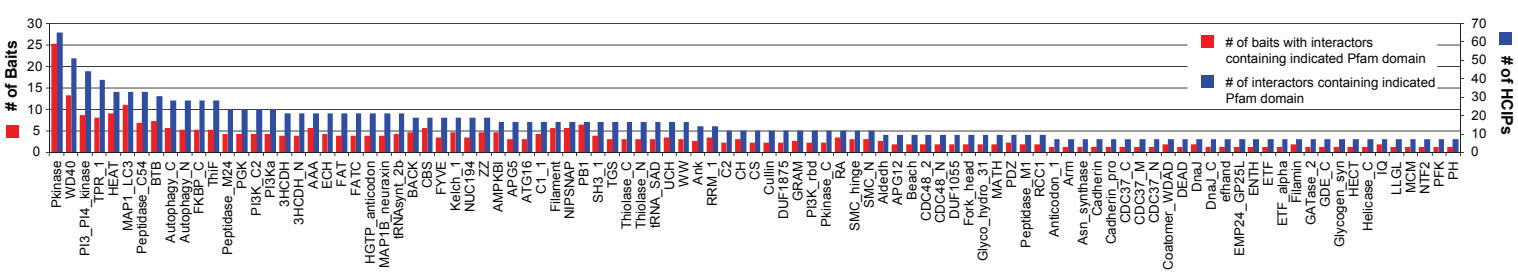

Supplementary Fig. S5d

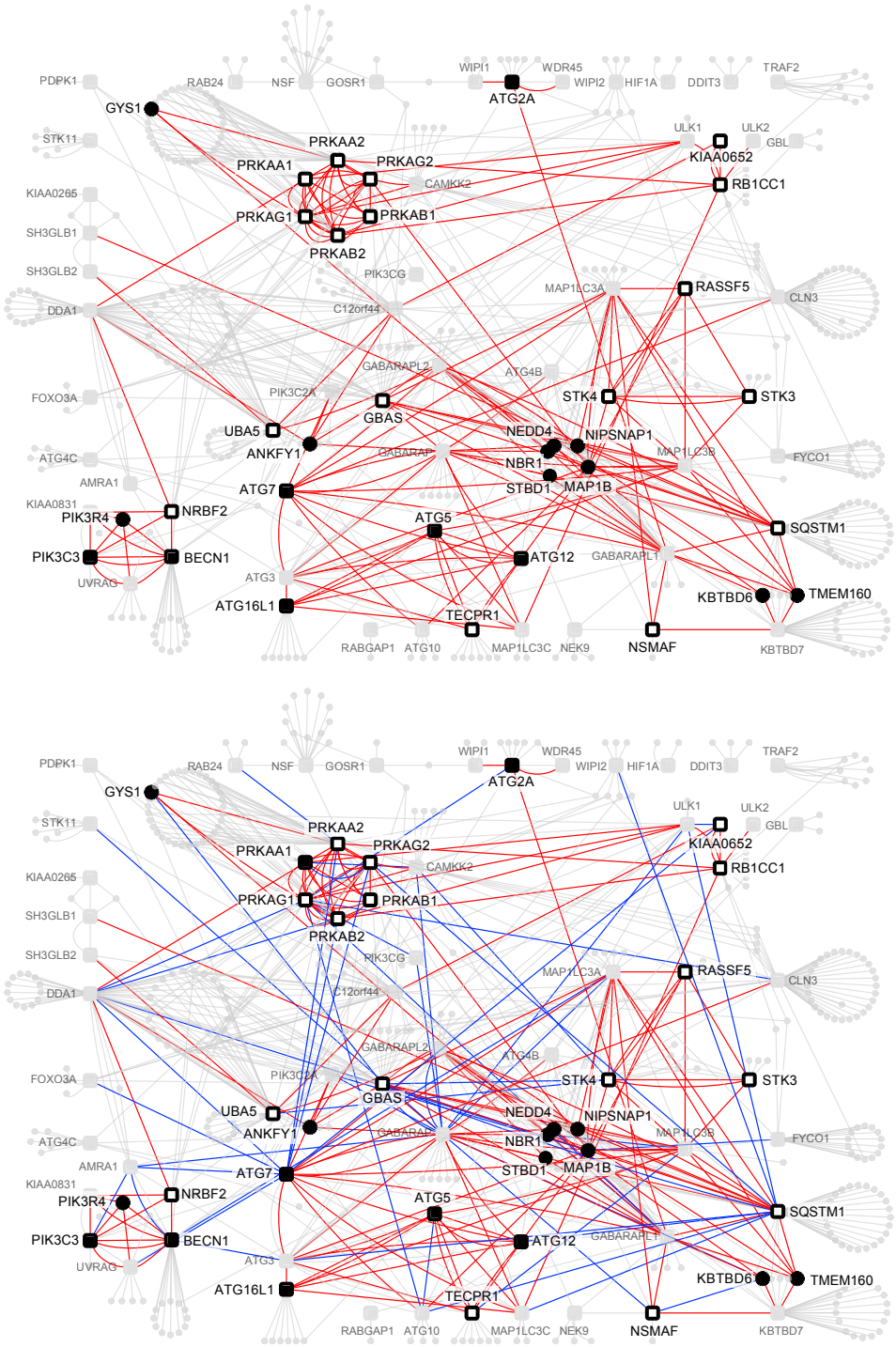

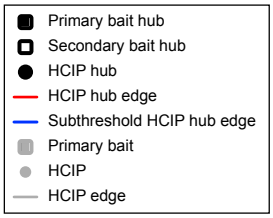

Supplementary Fig. S6

a

	Bait	HCIPs	Total known PPIs for bait (MINT/BioGRID)	# of known PPIs identified in this study by LC-MS/MS	Novel PPIs	Reciprocal PPIs	
						Potential reciprocal PPIs	Observed reciprocal PPIs
UBL conjugation system	ATG3	15	3	3	12	10	7
	ATG4B	6	4	3	3	7	4
	ATG5	7	2	1	6	5	4
	ATG7	6	1	1	5	8	6
	ATG10	18	1	0	18	7	0
	ATG12	11	14	3	8	6	3
	ATG16L1	8	2	1	7	6	1
	TECPR1	12			12	3	3
	Total	83	27	12	71	52	28

b

Bait	Interactor	Method	Reference
ATG16L	IKBKG	HT-AC-MS	Bouwmeester 2004
ATG16L	ATG12	HT-AC-MS	Ewing 2008
ATG12	SF3A1	HT-AC-MS	Ewing 2008
ATG12	AUP1	HT-AC-MS	Ewing 2008
ATG12	ATG16L	HT-AC-MS	Ewing 2008
ATG12	SF3B1	HT-AC-MS	Ewing 2008
ATG12	ATG3	AC-W	Tanida 2002
ATG12	ATG10	HT-AC-MS	Ewing 2008
ATG12	ATG5	HT-AC-MS	Ewing 2008
ATG12	PTK2	Y2H	Rual 2005
ATG12	KRTAP4-12	Y2H	Rual 2005
ATG12	MDFI	Y2H	Rual 2005
ATG12	DHX36	HT-AC-MS	Ewing 2008
ATG12	OTUD4	HT-AC-MS	Ewing 2008
ATG12	PLSCR1	Y2H	Rual 2005
ATG3	ATG12	AC-W	Tanida 2002
ATG3	ATG7	AC-W	Tanida 2002
ATG3	GABARAPL2	HT-AC-MS	Ewing 2008
ATG7	atg3	AC-W	Tanida 2002
ATG10	ATG12	HT-AC-MS	Ewing 2008
ATG5	ATG12	HT-AC-MS	Ewing 2008
ATG5	IMPDH2	HT-AC-MS	Ewing 2008
ATG4B	GABARAPL2	HT-AC-MS	Ewing 2008
ATG4B	fbxw11	HT-AC-MS	Sowa 2009
ATG4B	GABARAP	Y2H	Steizl 2005
ATG4B	MAP1LC3B	Y2H	Steizl 2005
ATG4B	C14orf139	Y2H	Steizl 2005

AC-W: affinity capture-western
Y2H: yeast 2 hybrid
HT-AC-MS: High-throughput affinity capture mass spec

c

Network	Potential reciprocal PPIs	Observed reciprocal PPIs
UBL conjugation system	44	21
ULK1 kinase	35	17
PIK3C3-BECN1	11	7
SH3GLB1	2	1
ATG2-WIPI	2	1
Total	94	47

Supplementary Fig. S6d

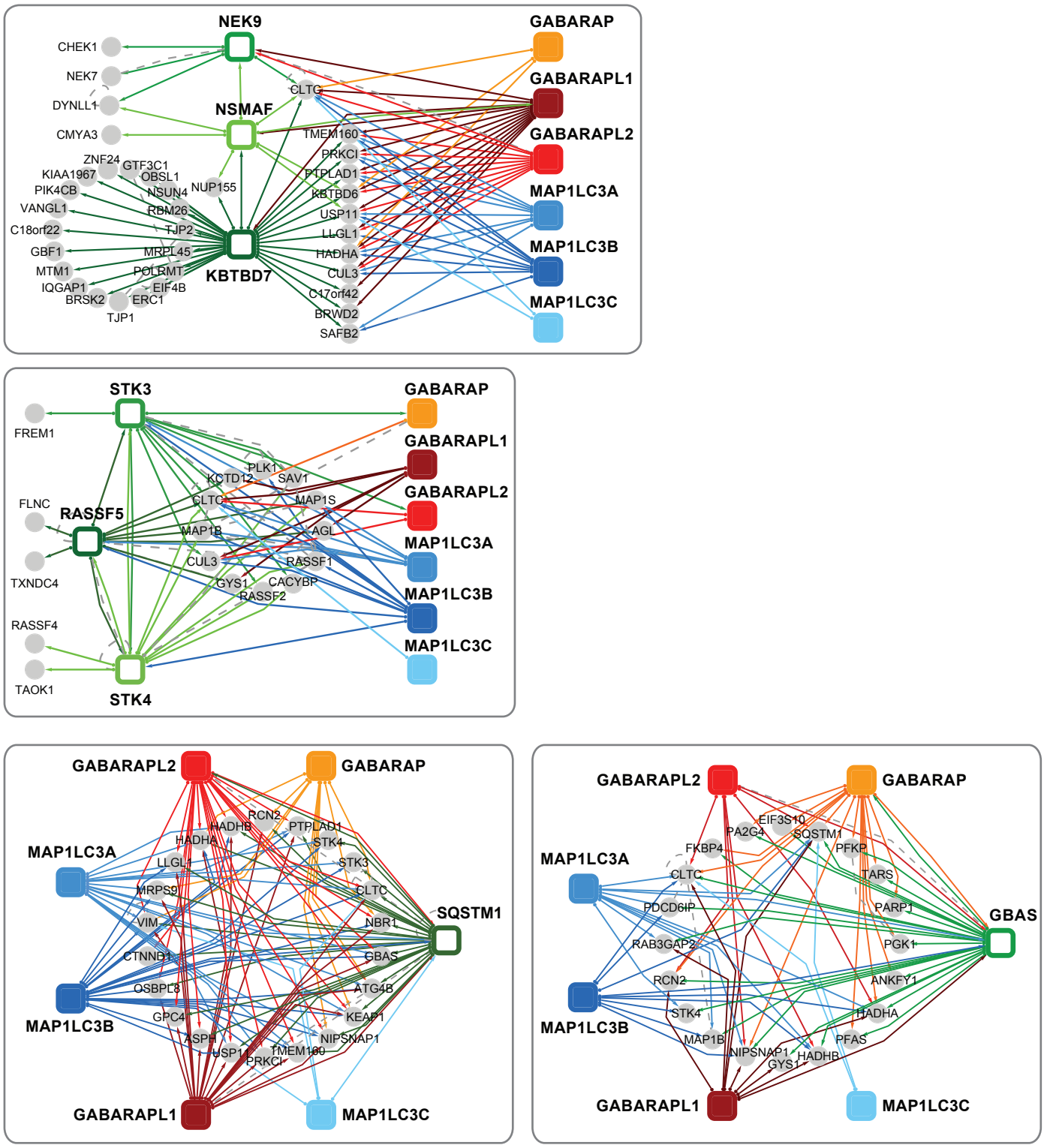

Primary bait (color coded)

Secondary bait (color coded)

HCIP

PPI database interaction

Supplementary Fig. S6e (Part 1)

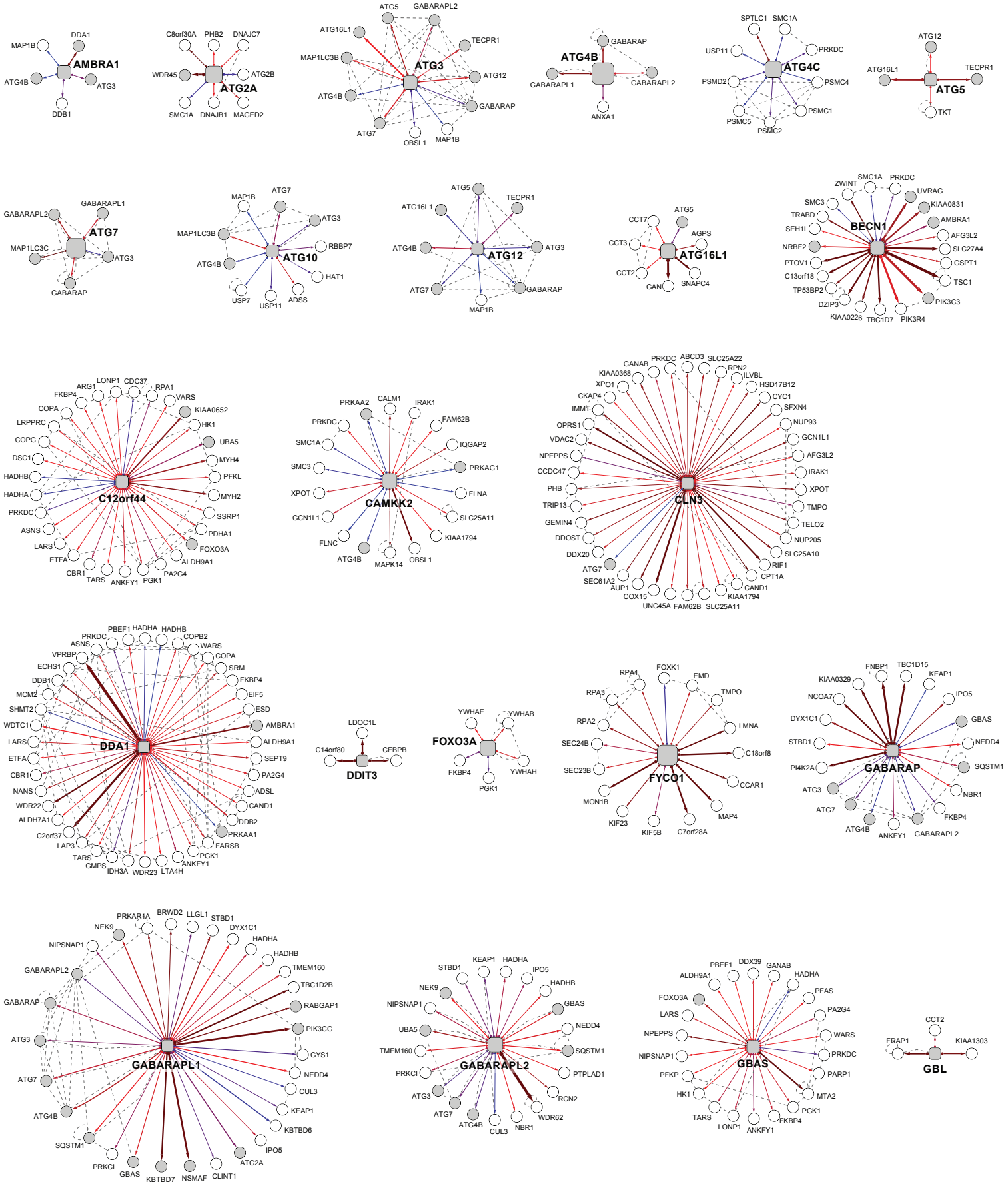

Supplementary Fig. S6e (Part 2)

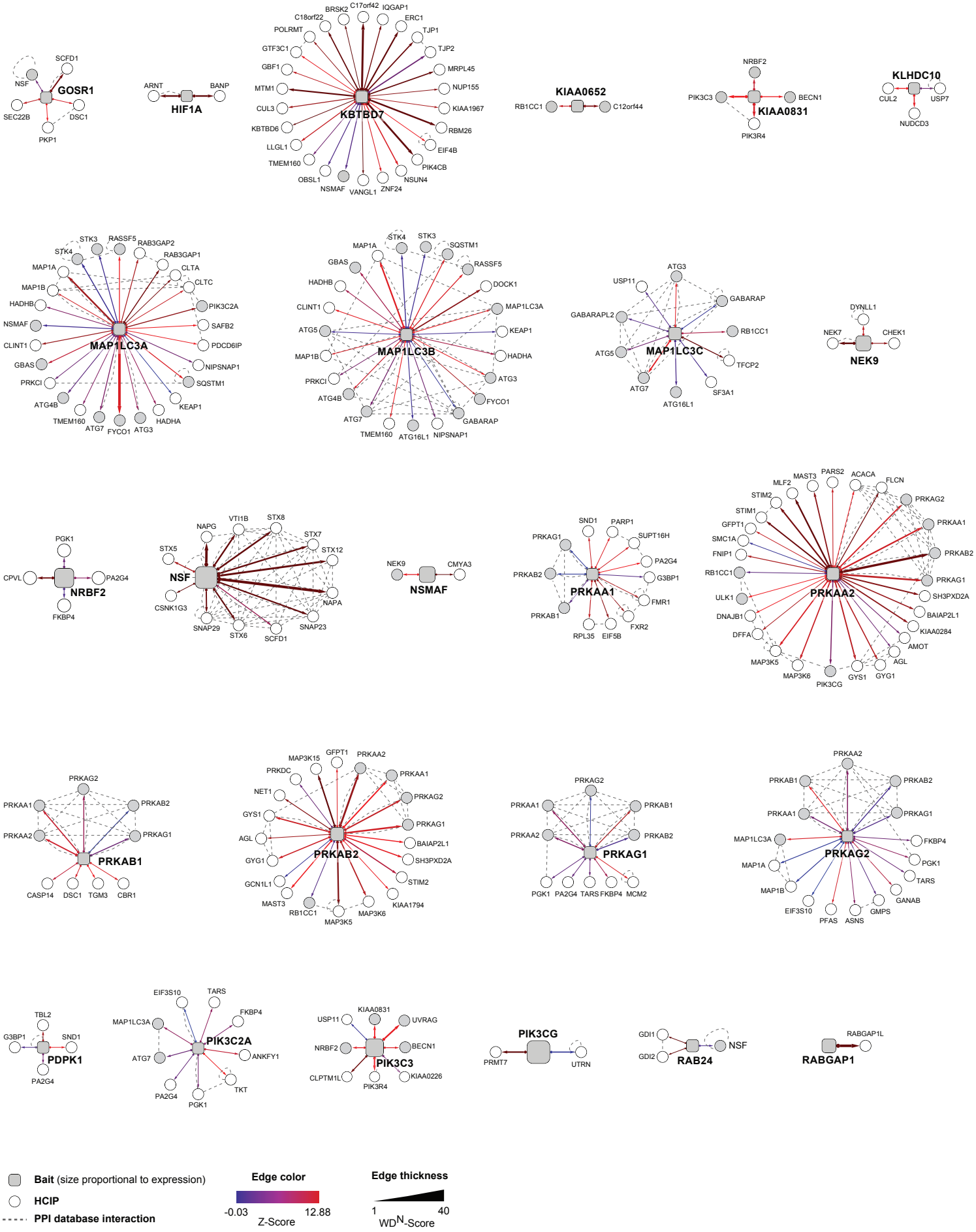

Supplementary Fig. S6e (part 3)

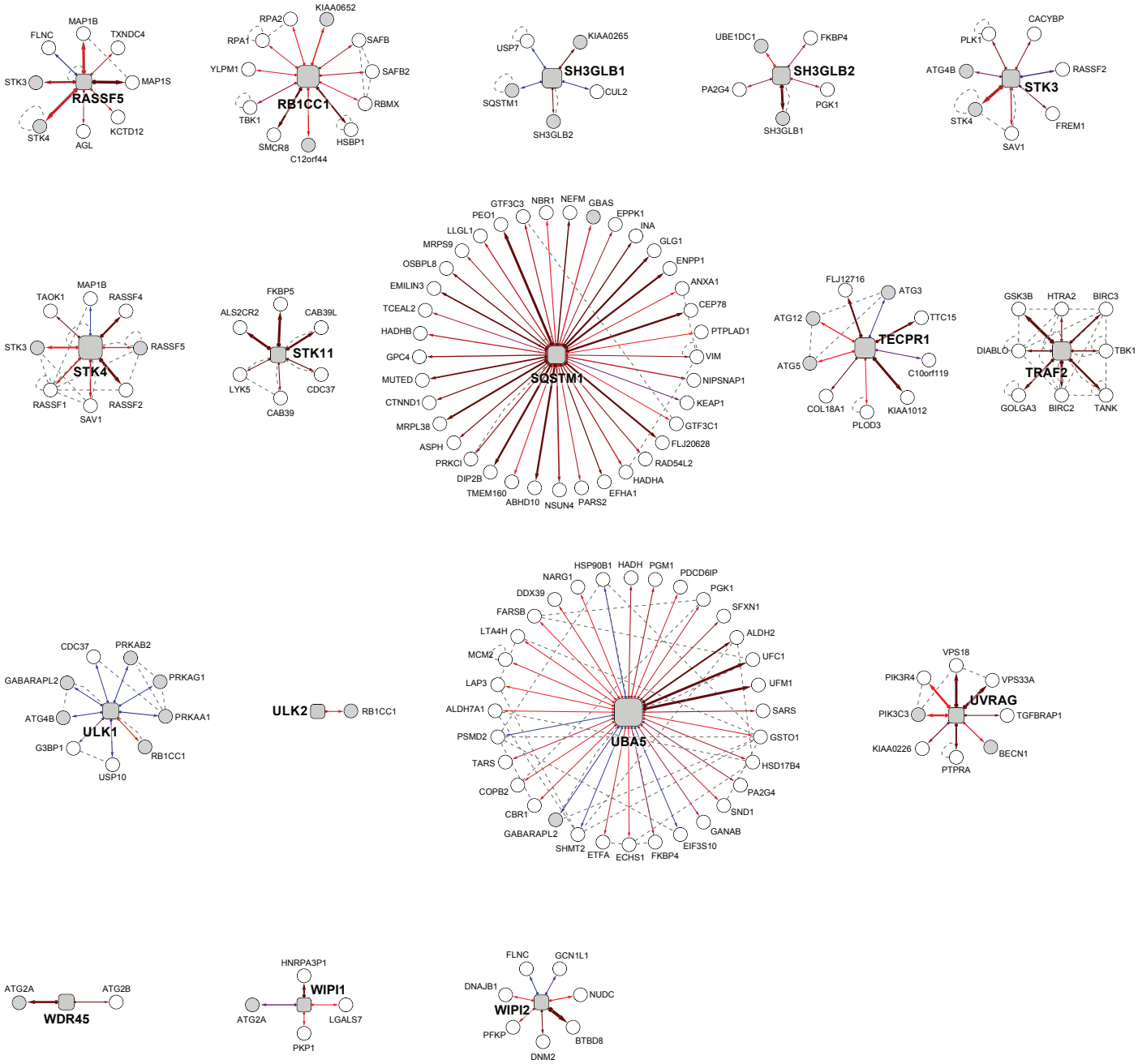

Supplementary Fig. S6f

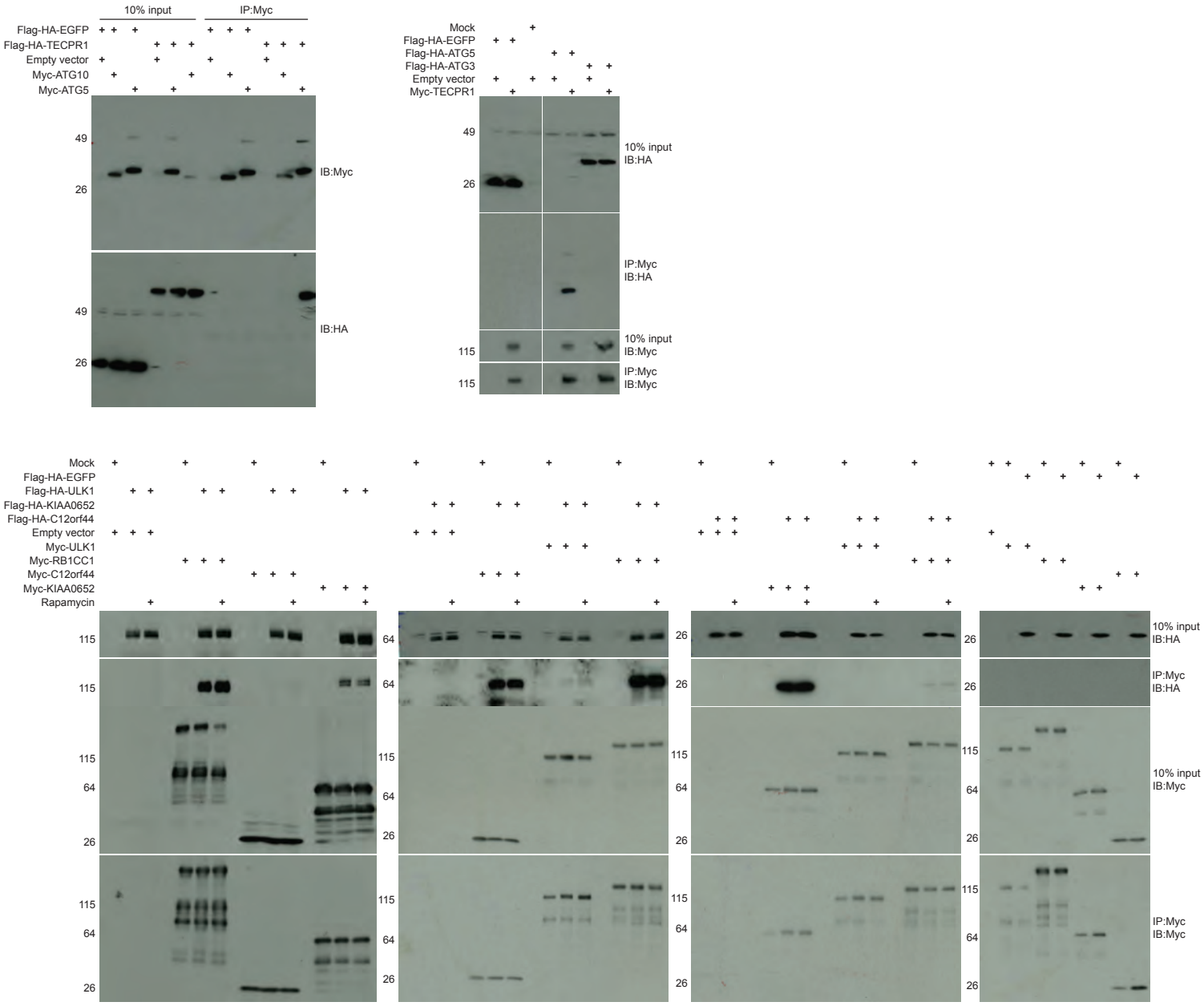

Supplementary Fig. S6g

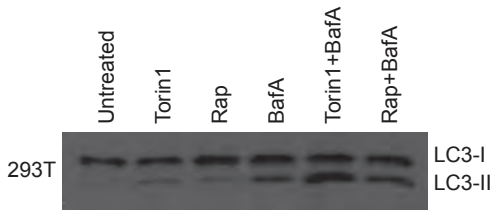

Supplementary Fig. S7

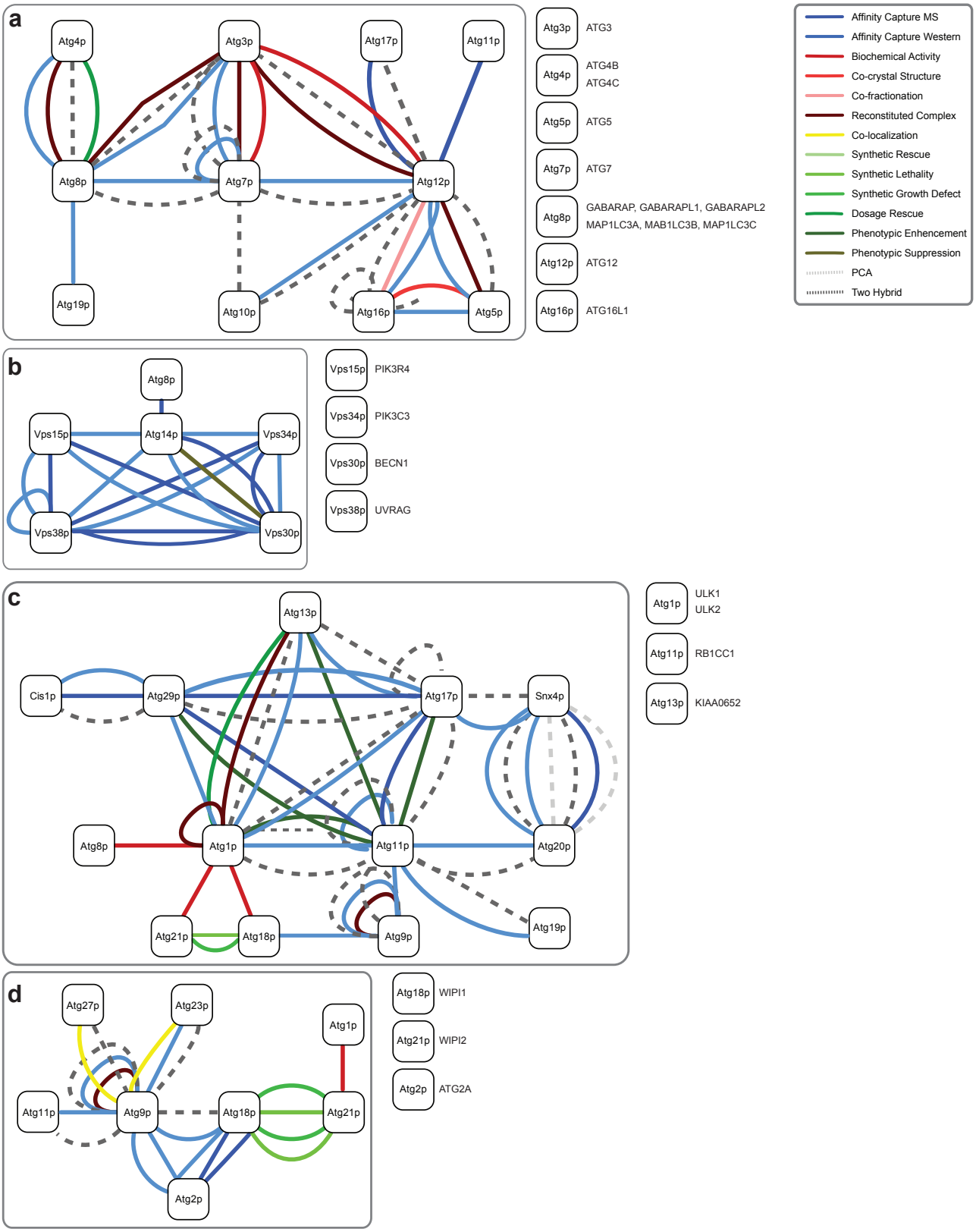

Supplementary Fig. S8

a

	Bait	HCIPs	Total known PPIs for bait (MINT/BioGRID)	# of known PPIs identified in this study by LC-MS/MS	Novel PPIs	Reciprocal PPIs		HCIPs found in biological replicate
						Potential reciprocal PPIs	Observed reciprocal PPIs	
Human ATG8's	GABARAPL1	40	3	1	39	10	4	26
	GABARAPL2	31	22	5	26	10	7	26
	GABARAP	27	13	1	26	12	6	19
	MAP1LC3A	35	7	2	33	11	4	22
	MAP1LC3B	34	3	1	33	13	4	29
	MAP1LC3C	15			15	9	1	13
	Total	182	48	10	172	65	26	135

b

Pfam domain	Gene Symbol					
WD40	BRWD2	NSMAF	WDR62	PIK3R4	LLGL1	ATG16L1
MAP1_LC3	GABARAP	GABARAP1	GABARAPL2	MAB1LC3B	MAB1LC3C	MAP1LC3A
Pkinase	NEK9	STK4	STK3	PRKCI	PIK3R4	
BTB	ANKFY1	KBTBD6	KBTBD7	KEAP1		
PI3_PI4_kinase	PIK3CG	PIK3C3	PIK3C2A	PI4K2A		
BACK	KBTBD6	KBTBD7	KEAP1			
Kelch_1	KBTBD6	KBTBD7	KEAP1			
PB1	SQSTM1	NBR1	PRKCI			
PI3K_C2	PIK3CG	PIK3C3	PIK3C2A			
PI3Ka	PIK3CG	PIK3C3	PIK3C2A			
TBC	TBC1D15	TBC1D2B	RABGAP1			
NIPSNAP	NIPSNAP1	GBAS				
ZZ	SQSTM1	NBR1				
C1_1	RASSF5	PRKCI				
ECH	HADHA					
FYVE	ANKFY1	FYCO1				
CS	DYX1C1	PTPLAD1				
PI3K_rbd	PIK3CG	PIK3C2A				
SH3_1	DOCK1	FNBP1				
TPR_1	DYX1C1	FKBP4				
Mst1_SARAH	STK4	STK3				
HEAT	RANBP5	PIK3R4				
Peptidase_C54	ATG4B					
3HCDH	HADHA					
3HCDH_N	HADHA					
C2	PIK3C2A					
Pkinase_C	PRKCI					
Thiolase_C	HADHB					
Thiolase_N	HADHB					
ENTH	CLINT1					
GRAM	NSMAF					
HECT	NEDD4					
WW	NEDD4					
Beach	NSMAF					
Cullin	CUL3					
MAP1B_neuraxin	MAP1B					
RA	RASSF5					
RCC1	NEK9					
UBA	SQSTM1					
Ank	ANKFY1					
BRO1	PDCD6IP					
Clathrin	CLTC					
Clathrin_lg_ch	CLTA					
Clathrin_propel	CLTC					
Clathrin-link	CLTC					
cNMP_binding	PRKAR1A					
CP2	TFCP2					
FCH	FNBP1					
FKBP_C	FKBP4					
Glycogen_syn	GYS1					
Hyd_WA	KIAA0329					
LLGL	LLGL1					
LysM	NCOA7					
PX	PIK3C2A					
Rlla	PRKAR1A					
RRM_1	SAFB2					
SAP	SAFB2					
Surp	SF3A1					
TLD	NCOA7					
ubiquitin	SF3A1					
UCH	USP11					
Ded_cyto	DOCK1					
PTPLA	PTPLAD1					
CBM_20	STBD1					
RUN domain	FYCO1					
DUF354	TBC1D15					
DUSP	USP11					
ThiF	UBE1DC1					
PRP21_like_P	SF3A1					
ATG_C	ATG2A					
Autophagy_N	ATG3					
Autophagy_act_C	ATG3					
Autophagy_Cterm	ATG3					
ATG11	RB1CC1					
DUF3694	RABGAP1					
PID	RABGAP1					
Cullin_Nedd8	CUL3					
APG5	ATG5					
ThiF	ATG7					
ATG16	ATG16L1					
PH	TBC1D2B					
No Domain annotation	TMEM160	MAP1A	RCN2	RAB3GAP2	RAB3GAP1	

Supplementary Fig. S9

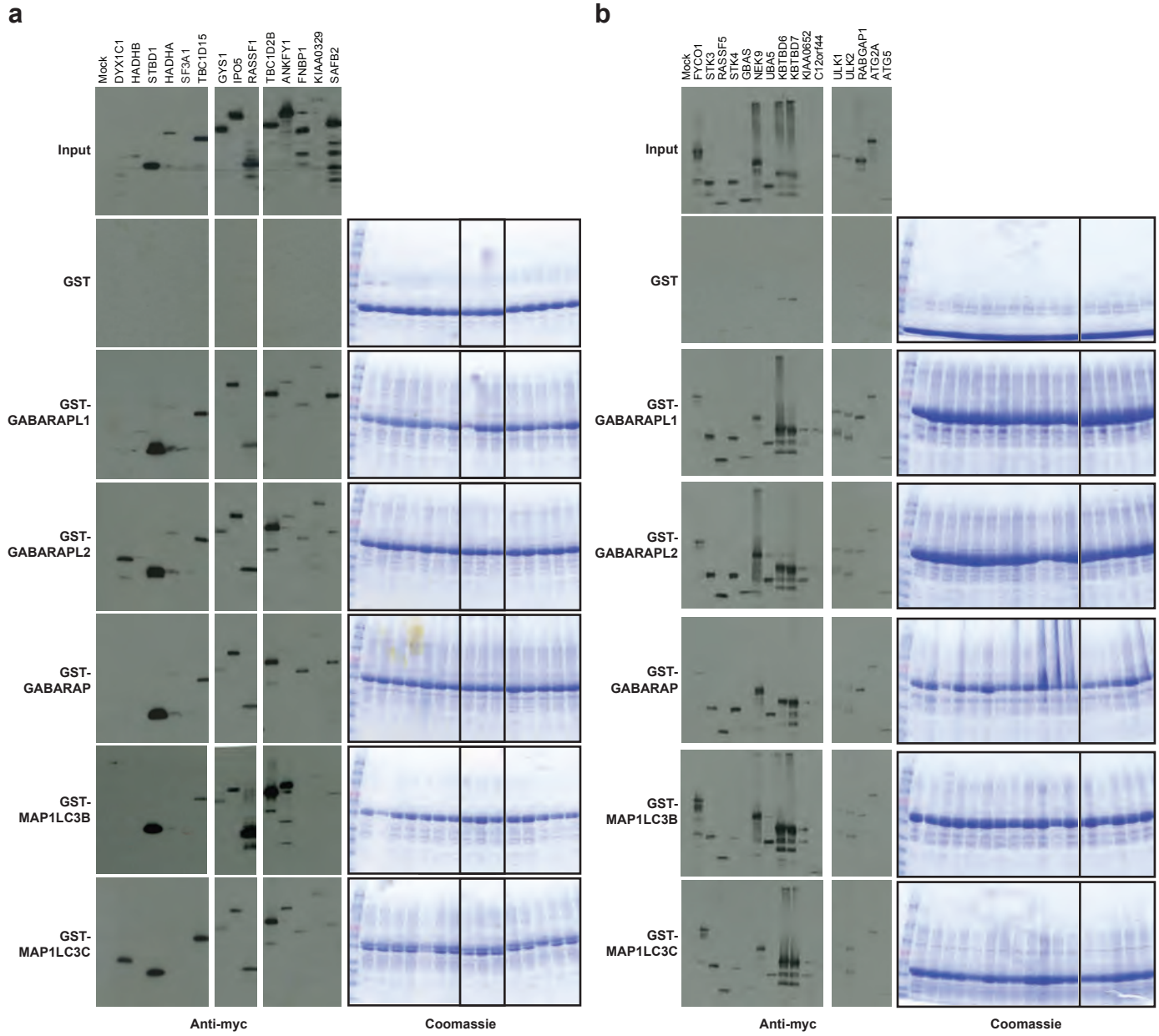

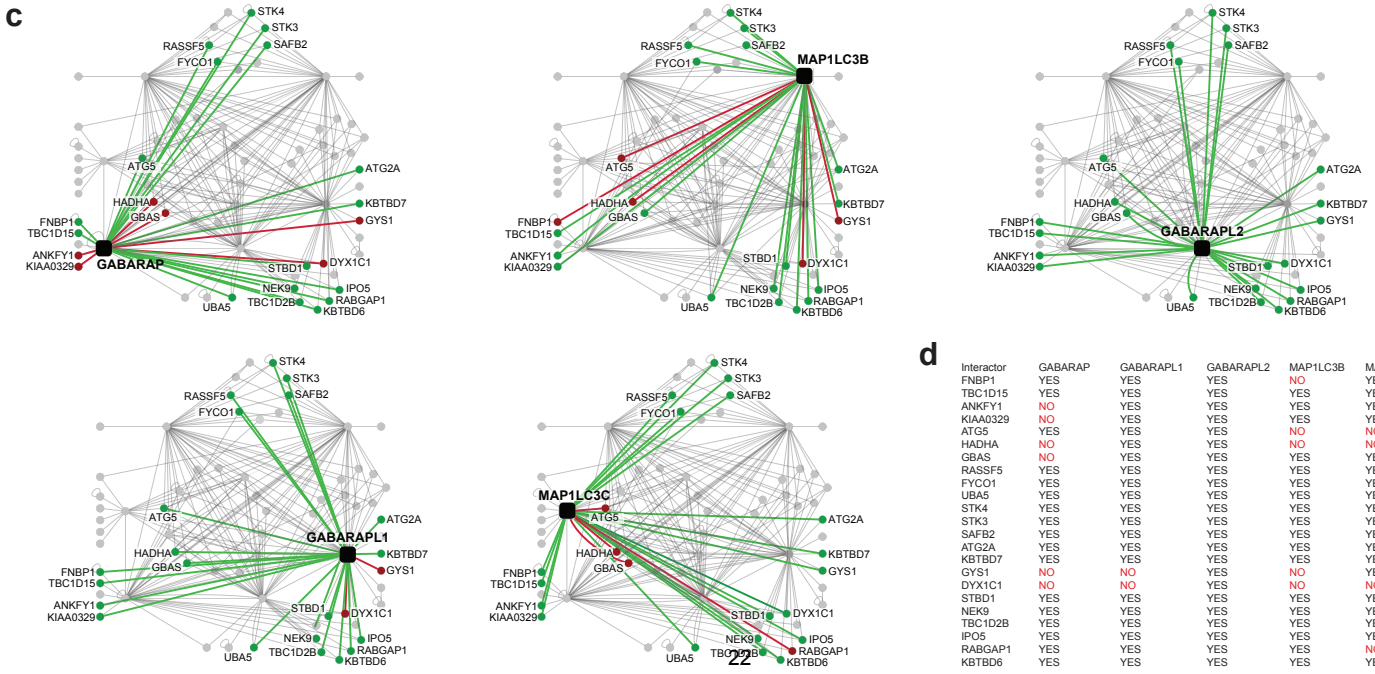

d

Interactor	GABARAP	GABARAPL1	GABARAPL2	MAP1LC3B	MAP1LC3C
FNBP1	YES	YES	YES	NO	YES
TBC1D15	YES	YES	YES	YES	YES
ANKFY1	NO	YES	YES	YES	YES
KIAA0329	NO	YES	YES	YES	YES
ATG5	YES	YES	YES	NO	NO
HADHA	NO	YES	YES	NO	NO
GBAS	NO	YES	YES	YES	YES
RASSF5	YES	YES	YES	YES	YES
FYCO1	YES	YES	YES	YES	YES
UBA5	YES	YES	YES	YES	YES
STK4	YES	YES	YES	YES	YES
STK3	YES	YES	YES	YES	YES
SAFB2	YES	YES	YES	YES	YES
ATG2A	YES	YES	YES	YES	YES
KBTBD7	YES	YES	YES	YES	YES
GYS1	NO	NO	YES	NO	YES
DYX1C1	NO	NO	YES	NO	NO
STBD1	YES	YES	YES	YES	YES
NEK9	YES	YES	YES	YES	YES
TBC1D2B	YES	YES	YES	YES	YES
IPO5	YES	YES	YES	YES	YES
RABGAP1	YES	YES	YES	YES	NO
KBTBD6	YES	YES	YES	YES	YES

Supplementary Fig. S10

a

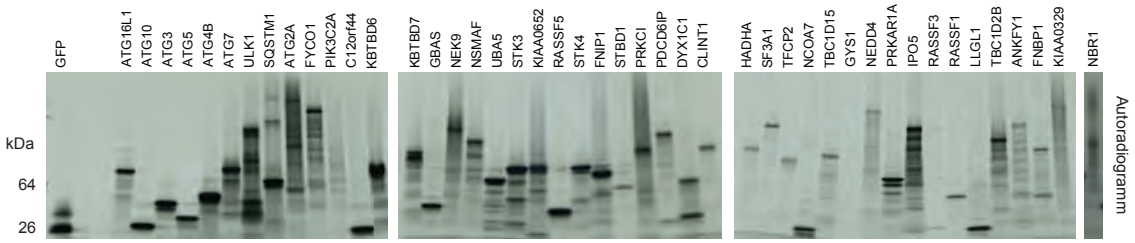

c

Interactor	GABARAP	GABARAPL1	GABARAPL2	MAP1LC3B	MAP1LC3C
ATG16L1	YES	YES	YES	YES	YES
TBC1D15	YES	YES	YES	YES	YES
KIAA0329	YES	YES	YES	YES	YES
RASSF5	YES	YES	YES	NO	NO
FYCO1	YES	YES	YES	YES	YES
NEDD4	YES	YES	YES	YES	YES
ATG4B	NO	NO	NO	YES	YES
STK3	YES	YES	YES	YES	YES
STK4	YES	YES	YES	YES	YES
ATG7	YES	YES	YES	YES	YES
NBR1	YES	YES	YES	YES	YES
SQSTM1	YES	YES	YES	YES	YES
ATG3	YES	YES	YES	NO	NO
GBAS	YES	YES	YES	YES	YES
UBA5	YES	YES	YES	YES	YES
PRKC1	YES	YES	YES	YES	YES
CLINT1	YES	YES	YES	YES	YES
DYX1C1	YES	YES	YES	NO	NO
STBD1	YES	YES	YES	YES	YES
NEK9	YES	YES	YES	YES	YES
NSMAF	YES	YES	YES	YES	YES
ATG2A	YES	YES	YES	YES	YES
KBTBD7	YES	YES	YES	YES	YES
GYS1	NO	NO	NO	NO	NO
PRKAR1A	YES	YES	YES	YES	YES
NCOA7	YES	YES	YES	YES	YES
IPO5	YES	YES	YES	NO	YES
KBTBD6	YES	YES	YES	YES	YES

b

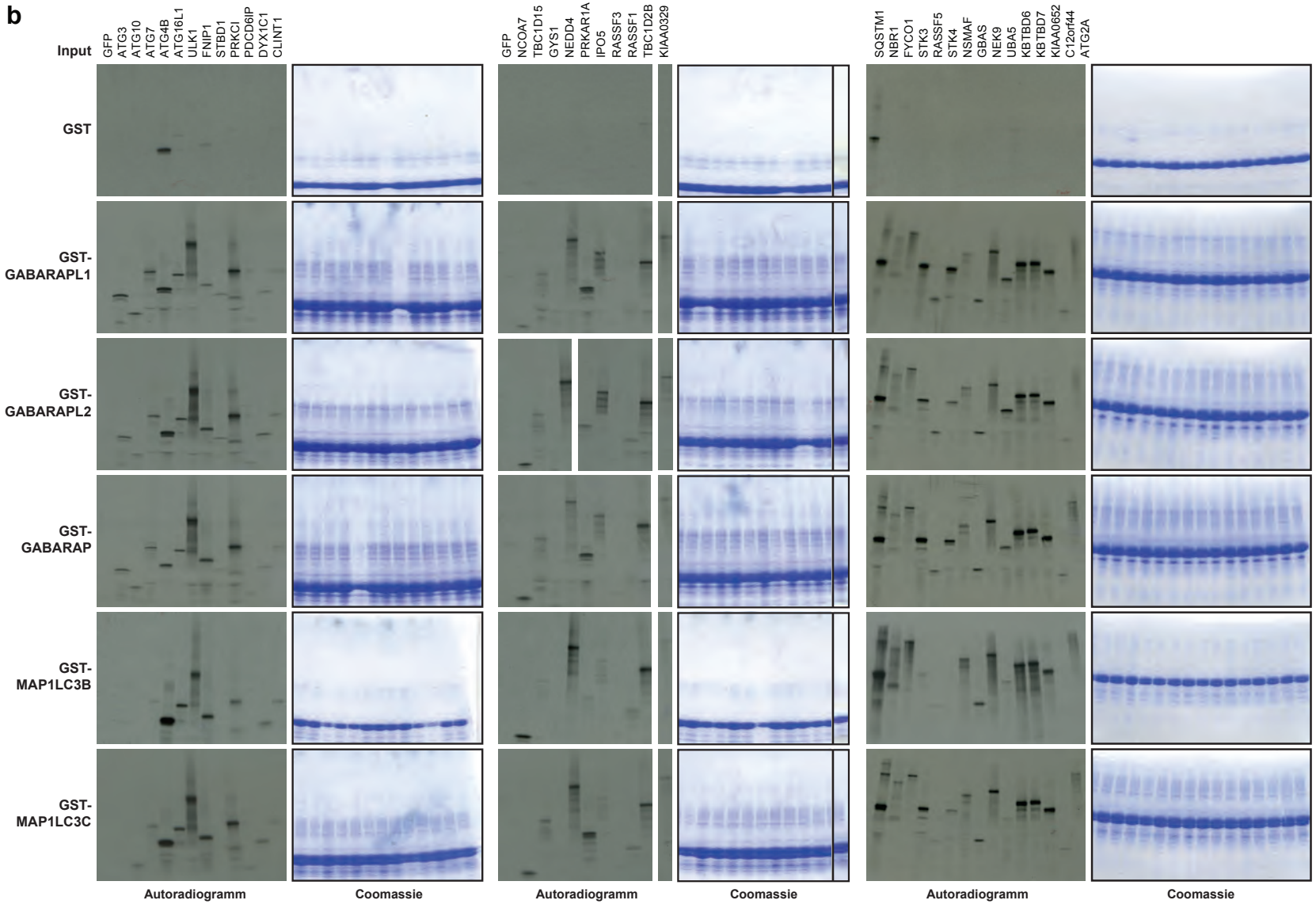

Supplementary Fig. S11a

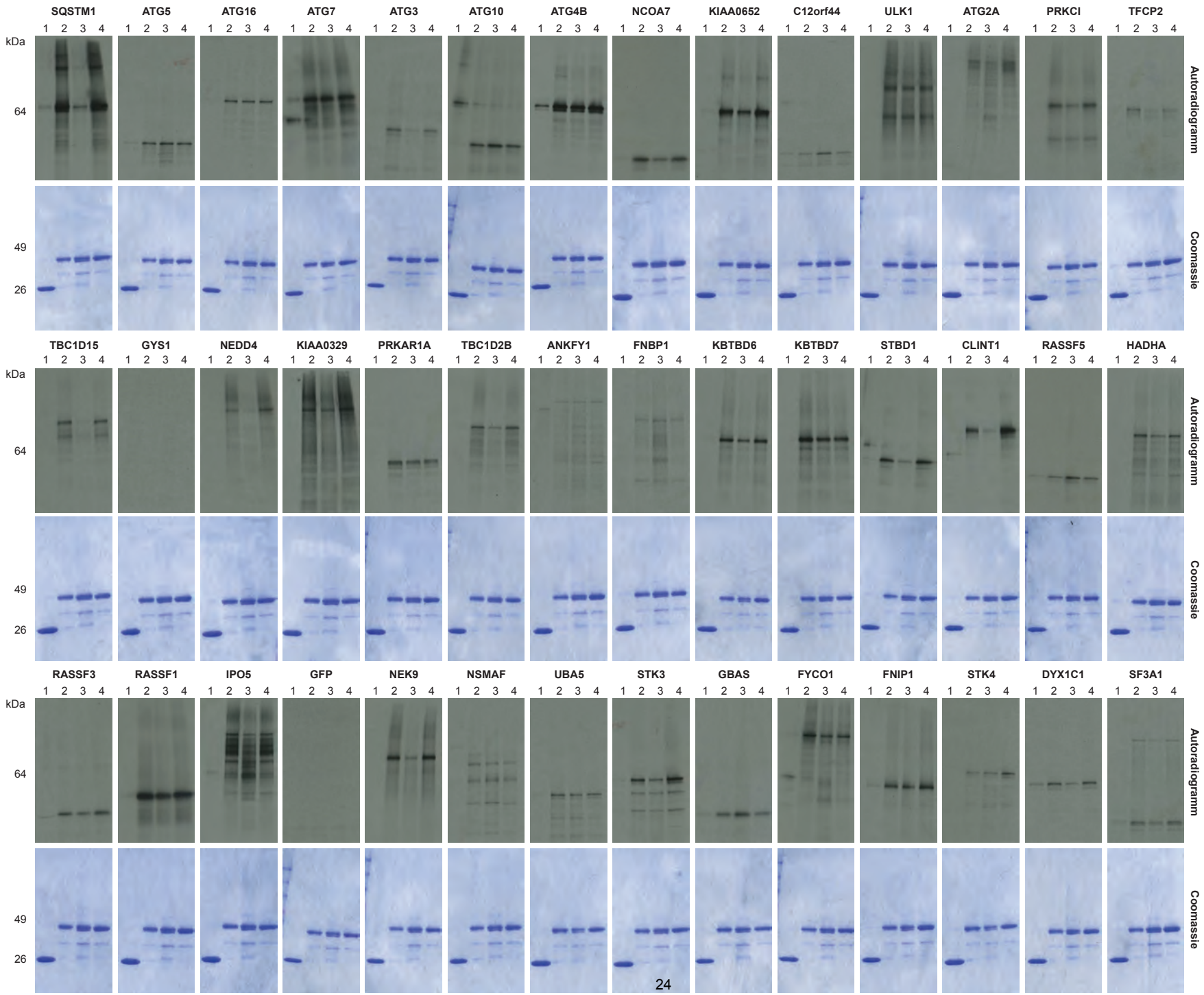

Supplementary Fig. S11b

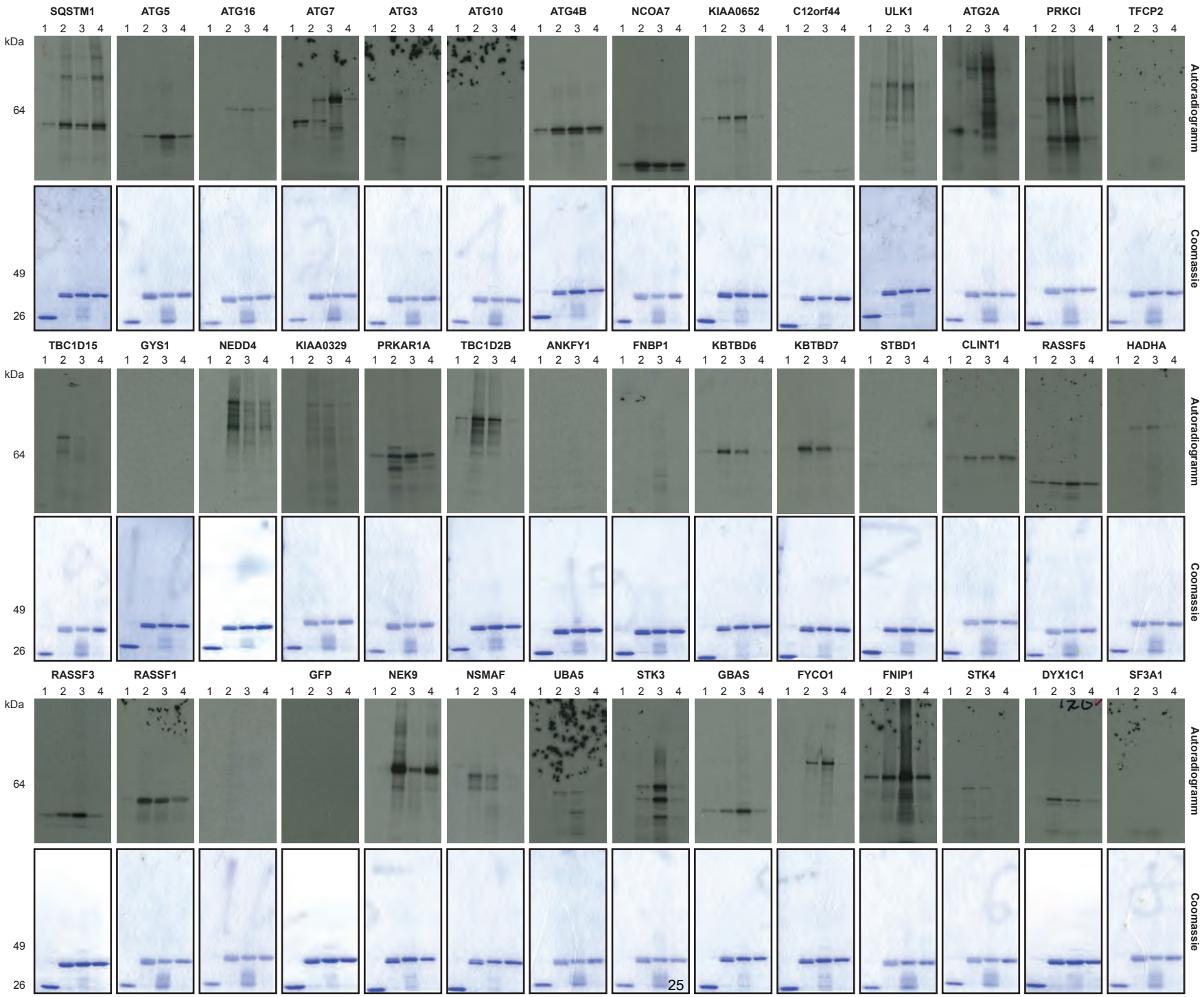

Supplementary Fig. S11c

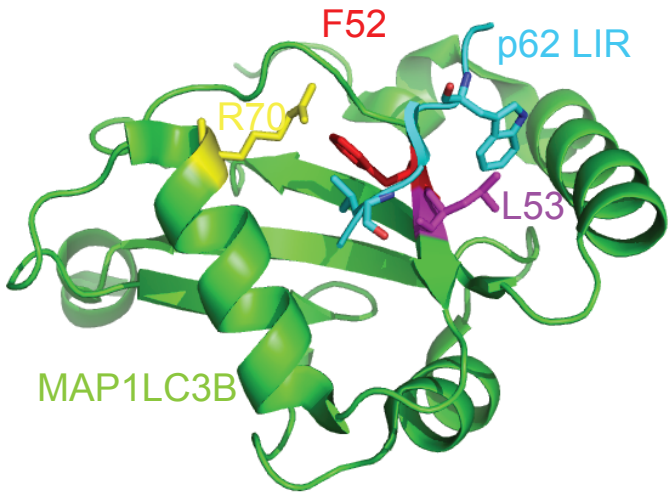

Supplementary Fig. S11d

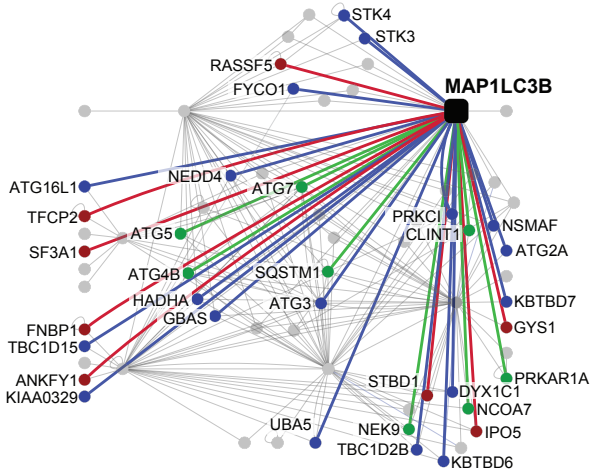

	Binding dependent on	
	Y52A/L53A	R70A
MAP1LC3B	ATG3	ATG3
	DYX1C1	DYX1C1
	KBTBD6	KBTBD6
	KBTBD7	KBTBD7
	NEDD4	NEDD4
	NSMAF	NSMAF
	TBC1D15	TBC1D15
	NEK9	
	SQSTM1	
		ATG16L1
		ATG2A
		FYCO1
		GBAS
		HADHA
		KIAA0329
		PRKCI
		STK3
		STK4
		TBC1D2B
		UBA5

Supplementary Fig. S11e

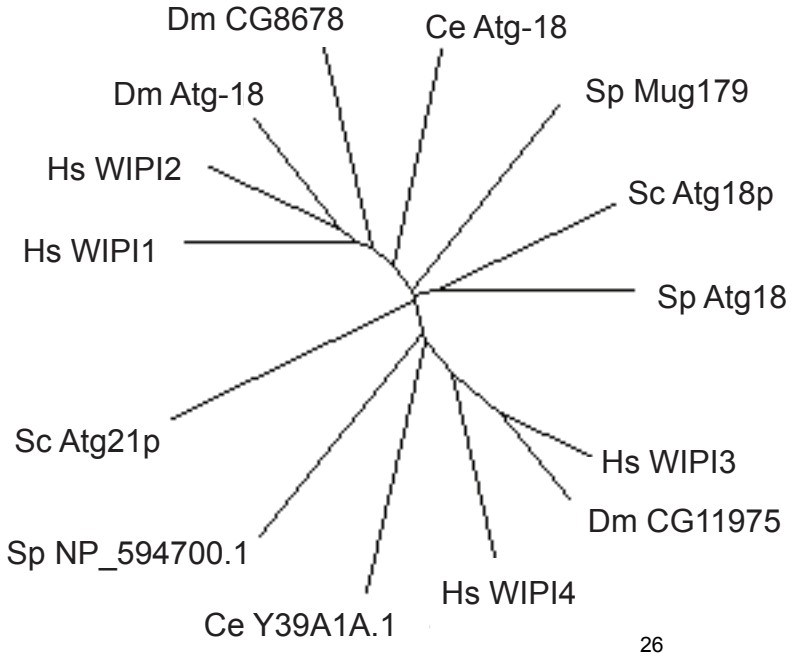

Supplementary Fig. S12

Delta Glycine					
HCIP/BAIT	GABARAP	GABARAPL1	GABARAPL2	MAP1LC3B	MAP1LC3A
ANKFY1			-4.68		
ATG16L1			-5.68		
ATG3	-7.72	-7.89	-8.16	-10.09	-8.02
ATG4B	11.60	12.95	-7.76	-6.45	9.64
ATG5					
ATG7	-10.97	-10.74	-9.87	-9.94	-10.56
BRWD2		-4.92			5.06
CLINT1					8.03
CLTA					7.54
CLTC	6.26	-5.23	-5.75	-5.61	8.85
CUL3	-6.01	-6.60	-3.51		5.73
DYX1C1	-4.36				
FYCO1				10.32	10.37
GABARAP		-8.16	6.50		-8.44
GABARAPL2	5.82	9.51			-8.44
GBAS	-9.70	7.87	-5.79	8.48	9.47
GYS1	-8.11	-3.38	-7.71		
HADHA		-4.79			
HADHB	-9.70	-6.09	7.04	9.35	9.20
KBTBD6	-9.85	-8.82	2.93	9.33	8.74
KEAP1	2.29	-4.79	5.25		
LLGL1	-7.87	4.51	7.41	7.50	6.42
MAP1A					
MAP1B	-4.95		4.59		5.26
MAP1LC3A				-6.28	-6.99
MAP1LC3B			4.69	-8.18	8.57
MAP1LC3C			7.68	8.67	
NBR1	7.95	8.24			
NCOA7		-4.22	6.19		
NEDD4	-6.13	-5.30			
NEK9	-8.84	-8.12	-7.42		7.35
NIPSNAP1	-7.21	-5.93	-6.56		6.38
NSMAF	-6.54	7.52	6.22	8.49	7.16
PDCD6IP	-5.75				7.06
PIK3C3					-5.54
PIK3R4					
PRKCI					
PTPLAD1	-5.64	4.64	5.74	8.20	7.09
RAB3GAP1	-8.05	-7.96	6.83	7.10	9.09
RAB3GAP2					5.36
RANBP5	-5.57				9.63
RASSF5	-8.31	-8.22	-7.19		
RB1CC1				-5.53	
RCN2					
SAFB2	-7.97	-7.80	-2.32		
SF3A1				-6.49	-7.74
SQSTM1					-4.68
STBD1	-10.72	-9.00	-8.00	9.89	8.60
STK3				-5.22	-10.19
STK4				-7.59	-7.39
TBC1D15	-5.58				
TBC1D2B		-6.47	-5.16		
TFCP2					
TMEM160	-10.63	-8.83	8.89	6.90	10.57
UBA5			6.94		
WDR62			8.52		

Supplementary Fig. S13

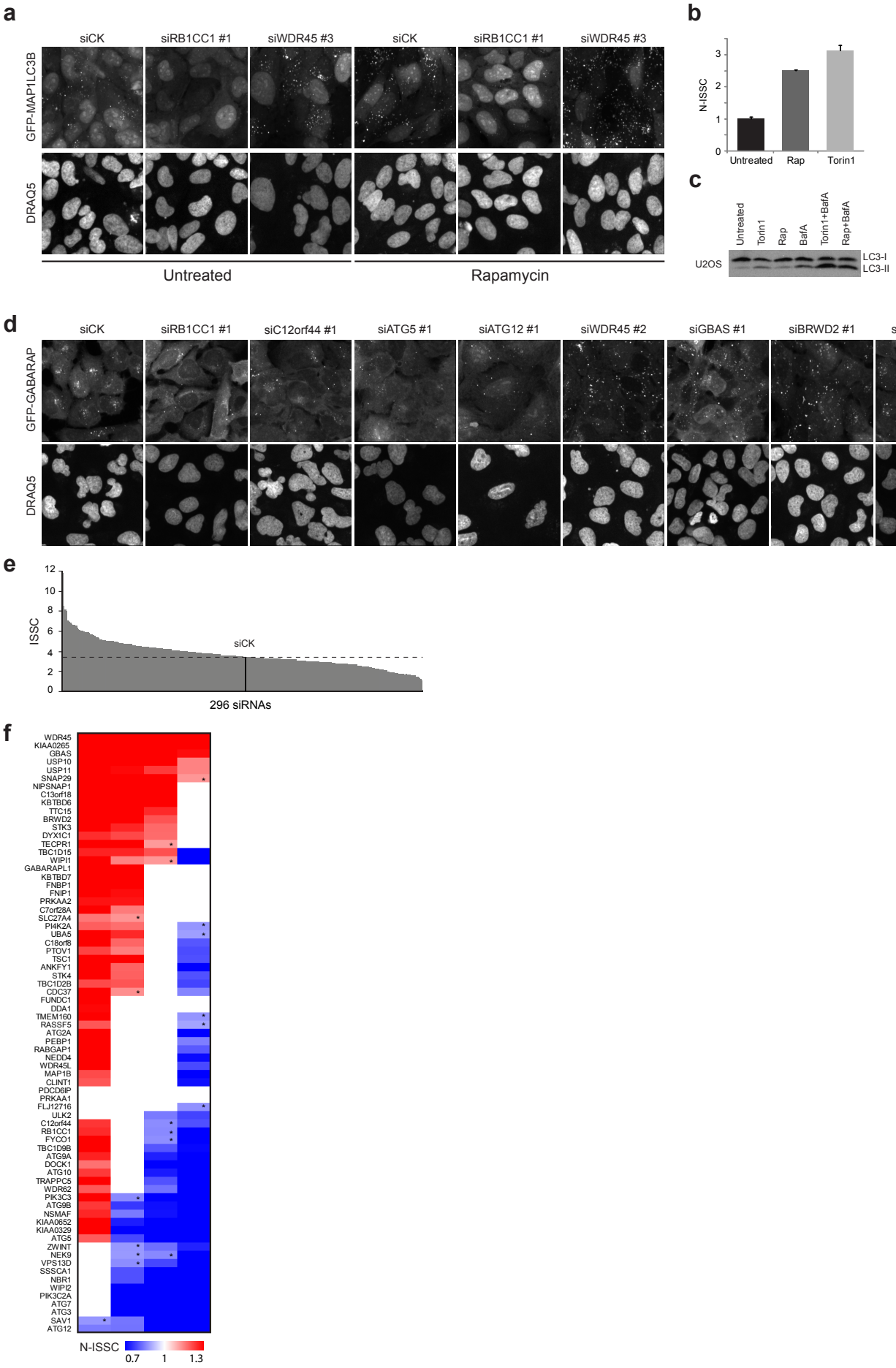

Supplementary Fig. S13g

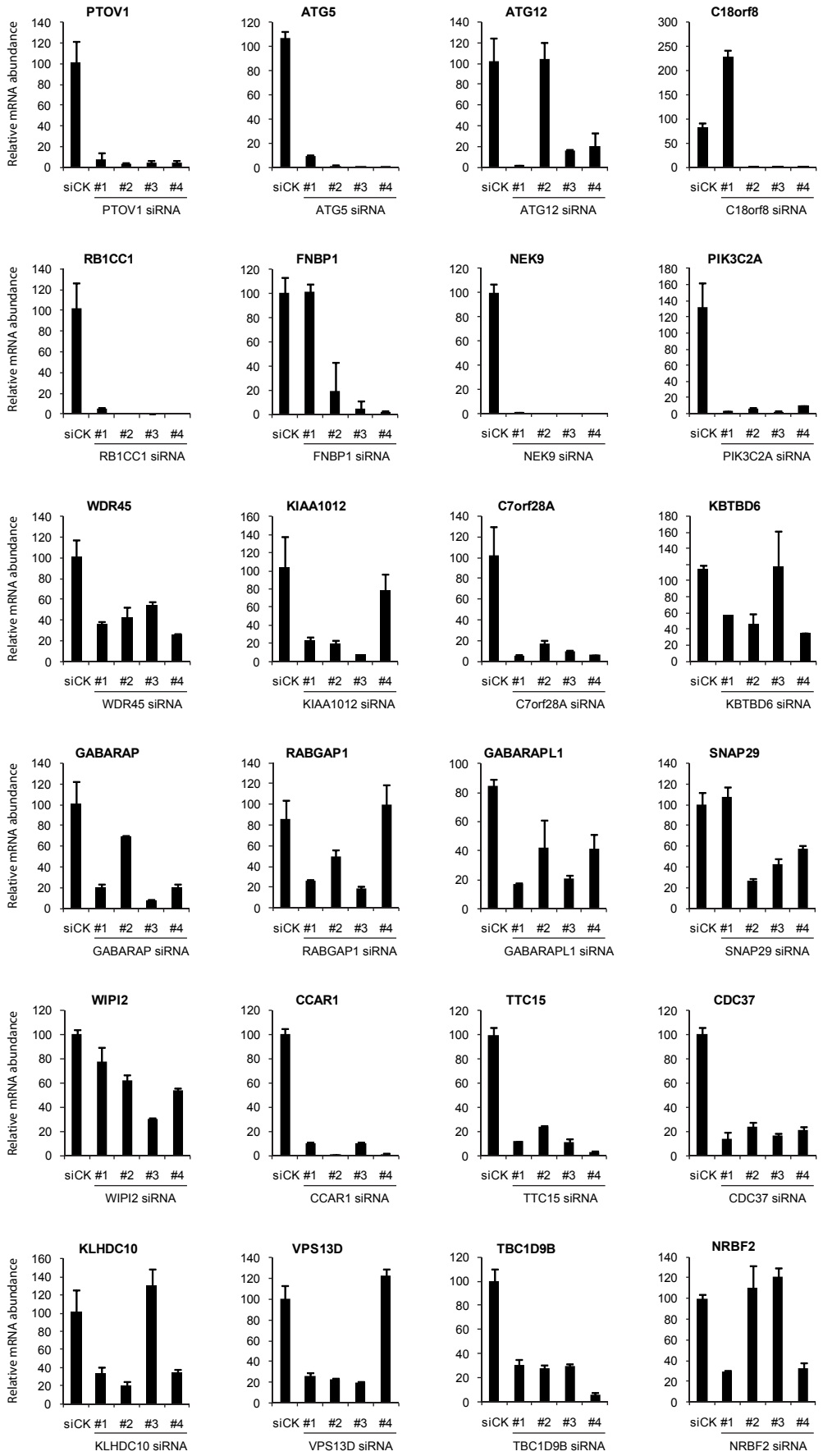

Supplementary Fig. S13h

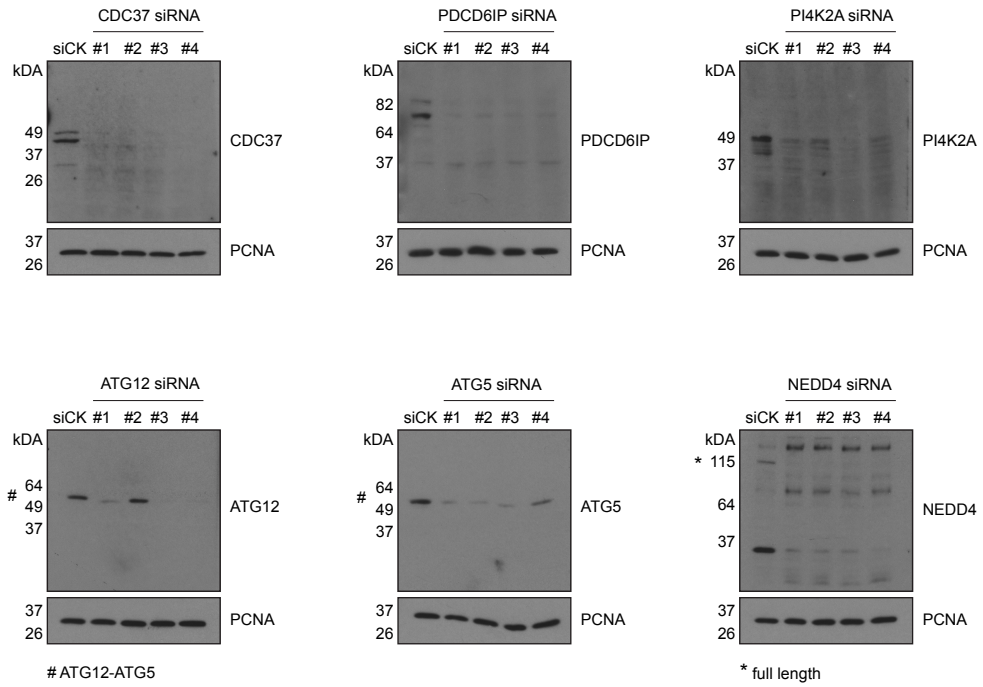

Supplementary Fig. S13i